This is an open access article published under a Creative Commons Non-Commercial No Derivative Works (CC-BY-NC-ND) Attribution License, which permits copying and redistribution of the article, and creation of adaptations, all for non-commercial purposes.

ACS Sustainable Chemistry & Engineering

pubs.acs.org/journal/ascecg

Research Article

Catalytic Conversion of Free Fatty Acids to Bio-Based Aromatics: A Model Investigation Using Oleic Acid and an H-ZSM-5/Al_2O_3 Catalyst

Songbo He, Frederike Gerda Hiltje Klein, Thomas Sjouke Kramer, Anshu Chandel, Zhuorigebatu Tegudeer, Andre Heeres, and Hero Jan Heeres*

Cite This: *ACS Sustainable Chem. Eng.* 2021, 9, 1128–1141

Read Online

ACCESS | Metrics & More | Article Recommendations | Supporting Information

ABSTRACT: The catalytic conversion of oleic acid to aromatics (benzene, toluene, and xylenes, BTX) over a granular H-ZSM-5/Al_2O_3 catalyst (ϕ 1.2−1.8 mm, 10 g loading) was investigated in a continuous bench-scale fixed-bed reactor (10 g oleic acid h^{-1}). A peak carbon yield of aromatics of 27.4% was obtained at a catalyst bed temperature of 550 °C and atmospheric pressure. BTX was the major aromatics formed (peak carbon yield was 22.7%), and a total BTX production of 1000 mg g^{-1} catalyst was achieved within a catalyst lifetime of 6.5 h for the fresh catalyst. The catalyst was deactivated due to severe coke deposition (*ca.* 22.1 wt % on the catalyst). The used catalyst was reactivated by an *ex situ* oxidative regeneration at 680 °C in air for 12 h. The regenerated catalyst was subsequently recycled, and in total, 7 cycles of reaction-regeneration were performed. A gradual decrease in the peak carbon yield of BTX was observed with reaction-regeneration cycles (*e.g.*, to 16.3% for the catalyst regenerated for 6 times). However, the catalyst lifetime was remarkably prolonged (*e.g.*, >24 h), leading to a significantly enhanced total BTX production (*e.g.*, 3000 mg g^{-1} catalyst in 24 h). The fresh, used, and regenerated catalysts were characterized by N_2 and Ar physisorption, XRD, HR-TEM-EDX, ^{27}Al, and ^{29}Si MAS ssNMR, NH_3-TPD, TGA, and CHN elemental analysis. Negligible changes in textural properties, crystalline structure, and framework occurred after one reaction-regeneration cycle, except for a slight decrease in acidity. However, dealumination of the H-ZSM-5 framework was observed after 7 cycles of reaction-regeneration, leading to a decrease in microporosity, crystallinity, and acidity. Apparently, these changes are not detrimental for catalyst activity, and actually, the lifetime of the catalyst increases, rationalized by considering that coke formation rates are retarded when the acidity is reduced.

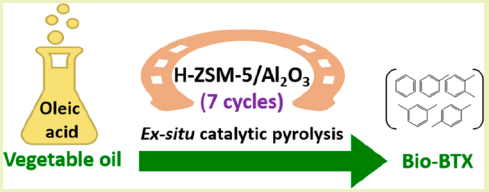

KEYWORDS: *Vegetable Oil, Fatty Acids, Oleic Acid, Bioaromatics, BTX, ZSM-5*

INTRODUCTION

Benzene, toluene, and xylenes (including *ortho-*, *meta-*, and *para*-xylene), also known as BTX, are the basic building blocks for a wide range of bulk chemicals, intermediates, and consumer products (*e.g.*, plastics, rubbers, resins, pharmaceuticals, cosmetics, ink, paints, thinners, and adhesives). Currently, catalytic reforming and steam reforming of naphtha represent the main source for aromatics production. The global BTX market was 162.7 billion dollars in 2018 and is forecast to reach 274.8 billion dollars by 2027.[1] However, traditional BTX production depends on the use of fossil feeds, and as such the prices of BTX are volatile and fluctuate (Figure S1). Besides, the production and use of fossil-based BTX (and derived products) result in CO_2 emissions. To overcome the drawbacks mentioned above, alternative technologies using renewable feedstocks to produce sustainable and bio-based aromatics have emerged and demonstrated in pilot and demo plants.[2]

One of the attractive technologies to obtain BTX from biomass is catalytic pyrolysis. Here, the biomass is heated to elevated temperatures, and the pyrolysis vapor is passed over an aromatization catalyst to obtain BTX. This concept is known as *ex situ* catalytic pyrolysis, which has been demonstrated by Bio-BTX BV, The Netherlands, since September 2019.[3] Alternatively, an *in situ* catalytic pyrolysis may be applied, in which case the aromatization catalyst is present in the pyrolysis reactor. This catalytic fast pyrolysis process has been under demonstration by Anellotech, USA, since March 2018.[4]

Numerous lignocellulosic biomass feedstocks (*e.g.*, pinewood[5]), as well as individual fractions thereof (cellulose,[6] hemicellulose,[7] and lignin[8]) and model compounds (*e.g.*, glucose,[9] xylitol[10]) have been used as input for catalytic pyrolysis to obtain bioaromatics. Nevertheless, due to the high oxygen content and the presence of minerals in lignocellulosic biomass, particularly relevant when using the *in situ* approach, the techno-economic viability of the use of solid woody biomass fro BTX production is still under debate. Significant achievements have also been realized in the catalytic upgrading

Received: August 23, 2020
Revised: November 18, 2020
Published: January 11, 2021

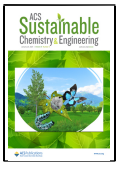

ACS Publications

© 2021 American Chemical Society

Table 1. State-of-the-Art of Bio-Based Aromatics from Vegetable Oils

	feedstock	reactor, catalyst and reaction conditions	aromatics maximum production[a]	ref
		Continuous Setups		
1	Peanut oil soap stock	Fixed bed reactor (*catalytic*), continuous, H-ZSM-5 catalyst: 15 g, feed: WHSV of 5.4 h^{-1}, T: 450−550 °C, TOS: 30 min	BTEX[b]: *ca.* 33 vol % (at 500 °C).	Hilten et al., (2011)[34]
2	Palm fatty acid distillate	Fixed bed reactor (*catalytic*), continuous, H-ZSM-5 and Ga, and Zn modifided H-ZSM-5 catalyst, feed: WHSV of 5 h^{-1}, T: 500 °C, TOS: 3 h	BTEX[b]: *ca.* 65 wt % (over 5% Zn/H-ZSM-5 at 500 °C).	Tamiyakul et al., (2016)[35]
3	Vegetable oils (3 types)	FCC plant (internal circulated riser-regenerator, *in situ catalytic*), continuous, E-Ultima FCC equilibrium catalyst, feed: 2.6 L h^{-1}, T: 550 °C, operation time: >6 h	Aromatics yield: 26.8 wt % (for rapeseed oil), 24.5 wt % (for soybean oil) and 22 wt % (for palm oil)	Bielansky et al., (2011)[36]
4	Camelina (sativa) seed oil	Fixed bed reactor (*ex situ catalytic*), continuous, Zn modified ZSM-5 catalyst: 25 g, feed: WHSV of 0.6 h^{-1}, T: 500 °C, TOS: 12 h	BTX[b] yield: *ca.* 6.2 wt % (over 20%Zn/ZSM-5)	Zhao et al., (2015)[37]
5	Soybean oil	Fixed bed reactor (*catalytic*), continuous, La−Fe modified Si-MCM-41 catalysts: 5 g, feed: 30 g with a WHSV of 6.69 h^{-1}, T: 460 °C	Aromatics: *ca.* 25 wt % (over Si-MCM-41)	Zheng et al., (2019)[38]
6	Canola oil	Fixed bed reactor (*catalytic*), continuous, H-ZSM-5, SiO_2, Al_2O_3 CaO and MgO catalysts: 2 g, feed: 5.1 g h^{-1} and 24.2 g h^{-1}, T: 400 and 500 °C	BTX[b] yield: 22.5 wt % (over H-ZSM-5 at 500 °C)	Idem, et al., (1997)[39]
7	Rapeseed oil	Fixed bed reactor (*catalytic*), continuous, Ga and Zn modified ZSM-5 catalysts: 0.25 g, feed: WHSV of 7.6 h^{-1}, T: 550 °C, TOS: 3 h	Aromatics: *ca.* 43 wt % of the overall product distribution (over Ga/ZSM-5)	Ramos et al., (2016)[40]
8	Rubber seed oil	Fixed bed reactor (*ex situ catalytic*), continuous, alkali treated ZSM-5 catalysts: 4 g, feed: WHSV of 1.37−6.85 h^{-1}, T: 400−700 °C, TOS: 15 min	BTX[b] selectivity: 78 A.% (at 550 °C and WHSV of 5.48 h^{-1}). Three cycles of reaction-regeneration	Wang et al., (2017)[41]
9	Oleic acid	Fixed bed reactor (*ex situ catalytic*), continuous, Al_2O_3, ZrO_2, AC, H-ZSM-5, HUSY, MCM-41 and Hβ catalysts: 1.2 g, feed: 0.25 mL h^{-1}, T: 500 °C, TOS: 30 min	Aromatics content: 65.2% (over H-ZSM-5)[c]	Zheng et al., (2020)[28]
10	Oleic acid	Microriser reactor, continuous, a commercial equilibrium catalyst, catalyst:feed = 4 (wt:wt), T: 480−585 °C	Aromatics concentration: *ca.* 30 wt % in C_5−C_{11} fraction	Dupain et al., (2007)[27]
11	Palm-oil-based fatty acids residue	Fixed bed reactor (*in situ catalytic*), continuous, H-ZSM-5, MCM-41, and their composites: 1 g, feed: WHSV of 2.5 h^{-1}, T: 450 °C	BTX[b] yield: *ca.* 23.6 wt % (over MCM-41-H-ZSM-5 (20/80 wt %) composite)	Ooi et al., (2005)[20]
12	Canola oil and its methyl ester	Fixed bed reactor (*in situ catalytic*), continuous, H-ZSM-5(50)[d], feed: WHSV of 2 h^{-1}, T: 450 °C	BTX[b] yield: *ca.* 25.8 wt % from canola oil, and 28.4 wt % from canola oil methyl ester	Bayat et al., (2015)[21]
13	Sunflower seed and meat oils	Fixed bed reactor (*in situ catalytic*), continuous, H-ZSM-5(30)[d] catalyst: 25 g, feed: LHSV of 2.5−3 h^{-1}, T: 450−550 °C	BTX (peak area% <1%) was not observed in the main products, though hydrocarbon content was high (*e.g.*, 63 peak area% at 500 °C)	Zhao et al., (2015)[42] and (2016)[43]
		Batch Setups		
14	Waste cooking oil	CDS Pyroprobe 5200 (*ex situ catalytic*), batch, alkali treated ZSM-5 catalyst: *ca.* 4 mg, feed: *ca.* 1 mg, T: 600 °C	BTXNE[b] selectivity: 58.6 A.%	Wang et al., (2017)[44]
15	Vegetable oils (3 types)	A 4-ml batch reactor, H-ZSM-5, feed: 150 mg, water: 0.1 g mL^{-1}, catalyst: 150 mg, T: 400 °C, P: 200 bar, reaction time: 180 min	BTX[b] yield: *ca.* 2.9 wt % from algal oil, 28.0 wt % from coconut oil, and 48 wt % from peanut oil	Mo et al., (2017)[22]
16	Palmitic acid	A 4-ml batch reactor, Zeolites Y, β, and H-ZSM-5 with different SiO_2/Al_2O_3 ratio, feed: 150 mg, water: 0.15 g mL^{-1}, catalyst: 150 mg, T: 400 °C, P: 240 bar, reaction time: 180 min	BTX[b] yield: *ca.* 43.9 C.% (over H-ZSM-5 (23)[d])	Mo et al., (2014)[30] and (2015)[31]
17	C_{18} fatty acids (3 types)	A 4 mL batch reactor, H-ZSM-5(30)[d], feed: 150 mg, water: 0.15 g mL^{-1}, catalyst: 150 mg, T: 400 °C, P: 240 bar, reaction time: 180 min	BTX[b] yield: *ca.* 12.5 C.% from linoleic acid, 23.1 C.% from oleic acid, and 30.8 C.% from stearic acid	Mo et al., (2015)[31]
18	Soybean oil	A 500 mL batch reactor, H-ZSM-5(23)[d], feed:catalyst: 4.5, T: 432 °C, reaction time: 12.5 min	BTEX[b] yield: *ca.* 7.6 wt %	Fegade et al., (2015)[45]
19	Soybean oil	A 500 mL batch reactor, H-ZSM-5(50)[d], feed: 200 mL, catalyst: 38 g, T: 430 °C, reaction time: 60 min	Aromatics: *ca.* 21 wt %	Kadrmas et al., (2015)[46]
20	Oleic acid	A microreactor (Quatra C-GC-MS), batch, H-ZSM-5(23)[d] catalyst: *ca.* 5−25 mg, feed: *ca.* 1 mg, T: 400 °C	BTX[b] yield: *ca.* 5 wt % (catalyst:oleic acid = 20).	Benson et al., (2008)[29]

[a]wt %: on weight basis, C.%: on carbon basis, A.%: on GC peak area basis, and vol %: on volume basis. [b]Abbreviated aromatics include benzene (B), toluene (T), xylene (X), naphthalene (N), and ethylbenzene (E). [c]Not clear whether this is for the total liquid phase or organic phase only. [d]SiO_2/Al_2O_3 molar ratio.

https://dx.doi.org/10.1021/acssuschemeng.0c06181
ACS Sustainable Chem. Eng. 2021, 9, 1128−1141

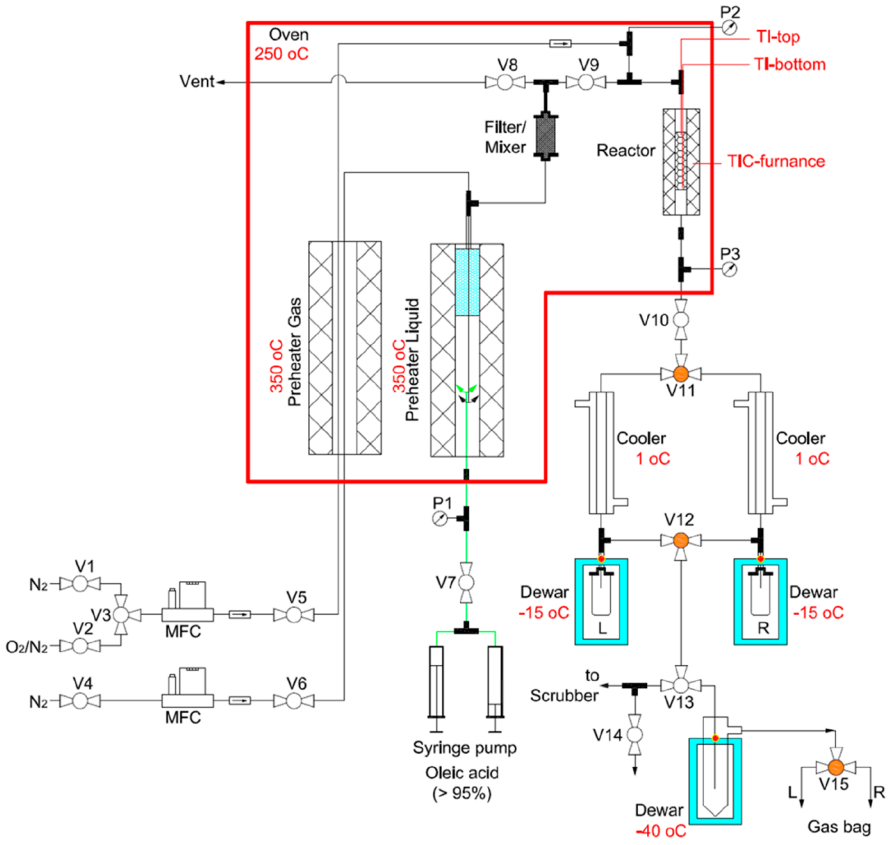

Figure 1. Schematic representation of the setup used for the catalytic conversion of oleic acid to bio-based aromatics.

of liquid biomass sources[11,12] like bioderived ethanol,[13] pyrolysis oils,[14] and model compounds (*e.g.*, furanics[15]) to BTX over various catalysts (*e.g.*, ZSM-5 zeolite[16]). Liquid industrial waste streams, such as black liquor[17] (from the pulp and paper industry) and crude glycerol[18] (from the biodiesel industry), have also been applied for bio-BTX synthesis. A continuous pilot plant for the conversion of crude glycerol using an acidic catalyst is currently in operation.[3]

The use of vegetable oils, preferably nonedible vegetable oils, (*e.g.*, Jatropha and Castor), has also been investigated for the production of bio-based fuels and chemicals in general[19] and BTX in particular. An overview of the catalytic conversion of vegetable oils to BTX is given in Table 1. A variety of catalysts (*e.g.*, Al_2O_3, modified H-ZSM-5 and MCM-41 zeolites, Table 1) have been screened for the conversion of vegetable oils (*e.g.*, palm oil, soybean, sunflower, and canola oil; Table 1) in various types of reactors at different scales (*e.g.*, in pyroprobes, fixed bed reactors, batch autoclaves, and FCC type of units; Table 1) at a wide range of temperatures (400−700 °C, Table 1) and pressures (1−240 bar, Table 1). BTX yields vary with the type of vegetable oil, *e.g.*, 23.6 wt % from palm oil residue,[20] 25.8 wt % from canola oil,[21] 28.0 wt % from coconut oil,[22] and 48 wt % from peanut oil.[22] This could be due to the differences in the fatty acid composition of the oils. Vegetable oils consist of various saturated and unsaturated fatty acids with carbon chain lengths between 8 and 60 (generally centered in the range of 16−18).[23−26] However, a comparison is difficult as different setups have been applied. The use of model compounds such as palmitic acid, oleic acid, linoleic acid, and stearic acid has also been investigated,[27−31] showing BTX yields of *ca.* 12.5 C.% from linoleic acid, 23.1 C.% from oleic acid, 30.8 C.% from stearic acid, and 43.9 C.% from palmitic acid under hydrothermal cracking condition (240 bar),[31] and 5 wt % from oleic acid under atmospheric cracking conditions.[29] Reaction pathways involving deoxygenation (decarboxylation, decarbonylation, and dehydration), cracking, cyclization, aromatization, alkylation, and polymerization have been proposed to explain the observed product portfolio.[29,32,33]

However, all of the reported studies using a continuous reactor configuration (*e.g.*, fixed bed reactor and mini-FCC plant; Table 1) did not consider the change in product selectivity with time on stream (TOS), productivity (aromatics or BTX production based on a unit catalyst weight or volume), catalyst stability (lifetime), and regenerability (reaction-deactivation-regeneration cycles) of the catalysts, which are of vital importance to determine the techno-economic potential of bio-BTX synthesis from vegetable oils. Besides, shaped H-ZSM-5 zeolite-based catalysts in combination with a binder, as used in this study, have not been considered, which is relevant for scale-up of the technology (*e.g.*, using FCC technology[37]). Furthermore, catalyst deactivation mechanisms when using vegetable oils are unclear. This is very relevant information for further studies on, *e.g.*, reactor and process optimization for enhanced aromatics production. Catalyst reuse in a batch reactor after a one-time reaction followed by drying and after two sequences involving reaction followed by an oxidative regeneration step has been studied, showing that catalyst deactivation occurred after a single use (related to a decrease in surface area and coke formation). Besides, irreversible catalyst deactivation occurred after one cycle of reaction-regeneration.[30,31]

In recent publications from our group using crude glycerol[18] and pure glycerol[47] as the feedstocks for bio-BTX production,

https://dx.doi.org/10.1021/acssuschemeng.0c06181
ACS Sustainable Chem. Eng. 2021, 9, 1128−1141

we have observed differences in BTX yields, indicating that plant oil residues (*e.g.*, free fatty acids and fatty acid methyl ester) in the crude glycerol may have a major effect on BTX yields and the rate of deactivation of the catalysts. As such, for the processing of crude glycerol, it is of interest and relevant to determine the effects of such residues on BTX yields in separate model studies in the absence of glycerol.

We here report studies on the catalytic pyrolysis of a representative model compound in the form of oleic acid for BTX synthesis. Oleic acid is a representative fatty acid and is present in its ester form in a variety of vegetable,[23−26] animal,[48] and fish[49,50] oils/lipids, with contents ranging 1.0−90.7%. In addition, it is known to be present in crude glycerol and waste vegetable oil streams (e.g., used frying oils). Granular alumina bonded H-ZSM-5 catalyst (H-ZSM-5/Al_2O_3) has been applied, considering that Al_2O_3 is a well-known binder in industrial catalysts (*e.g.*, FCC catalysts used in fluidized bed reactors[51]). Binders (*e.g.*, alumina, silica, and clay) are known to affect the performance of H-ZSM-5 based catalysts when used for the catalytic pyrolysis of biomass.[52] For instance, for Al_2O_3-bound ZSM-5 extrudates, additional Bronsted acid sites are reported to be formed,[53] which might be beneficial for aromatics production. Catalyst performance (aromatics yield and selectivity) of the catalytic aromatization of oleic acid with time on stream (TOS) and catalyst lifetime were evaluated in a continuous bench-scale reactor. An oxidative regeneration process was applied to reuse the catalyst and seven reaction-regeneration cycles were performed to investigate catalyst regenerability. In addition, the fresh, used, and regenerated catalysts were characterized in detail by various techniques to obtain insights into catalyst deactivation mechanisms. The product distributions over the active and deactivated catalysts were also determined to propose a reaction network for the conversion of free fatty acids to aromatics.

EXPERIMENTAL SECTION

Materials. A granular alumina bonded H-ZSM-5 catalyst (H-ZSM-5/Al_2O_3, 60/40 wt %, ϕ 1.2−1.8 mm) was produced at Yangzhou Baisheng Catalyst Co., Ltd., PR China. The SiO_2/Al_2O_3 molar ratio of the H-ZSM-5 zeolite was 28. The as-received H-ZSM-5/Al_2O_3 catalyst was heated to 600 °C with a heating rate of 1 °C min^{-1} followed by isothermal calcination for 8 h in a muffle furnace (LT 9/11/P330, Nabertherm GmbH). The calcined H-ZSM-5/Al_2O_3 catalyst (termed as Fresh catalyst) was stored in a vacuum desiccator (Bel-Art F42400−2141, BEL-ART - SP Scienceware & HB Instruments) filled with silica gel (Product No. 11418580, Fisher Scientific Nederlands).

The oleic acid (>95% purity, Product No. O/0200/17) was supplied by Fischer Scientific Netherlands. Ethanol, tetrahydrofuran (THF), and *n*-nonane were of analytical grade and supplied by Sigma-Aldrich. All gases (*e.g.*, N_2, He, and Ar, 99.999% purity) and liquid N_2 and Ar were supplied by Linde.

Catalytic Conversion of Oleic Acid. The catalytic conversion of oleic acid was performed in a bench-scale fixed bed reactor setup, which is schematically shown in Figure 1. The fresh H-ZSM-5/Al_2O_3 catalyst (10 g) was loaded to the isothermal zone of a stainless steel tubular reactor (1 × 0.083 in., length = 300 mm, Swagelok, part no. SS-T16-S-083-6ME). The rest of the reactor tube was filled with quartz wool (Part No. BEHRB00027716, VWR international). The reactor was then heated to 550 °C with a heating rate of 5 °C min^{-1} (controlled by a temperature controller, UR3274, Wachendorff Prozesstechnik GmbH & Co. KG) under an N_2 flow of 50 mL min^{-1} (controlled by a mass flow controller, MRH 469/2, Bronkhorst, The Netherlands). The as-received oleic acid was pumped (10 g h^{-1}) into a preheater (maintained at 350 °C) by a syringe pump (NE-1010, Prosense B.V.) using a gastight syringe (100 mL part no. 86020, Hamilton). The oleic acid vapor mixed with N_2 gas (50 mL min^{-1}) was first passed to the vent (to purge the preheater and transfer lines for ca. 2 h) and then introduced to the catalyst reactor (maintained at 550 °C) by switching on Valve V9 (Figure 1) and Valves V5 and V8 off (Figure 1). The reactions were performed at atmospheric pressure, a catalyst bed temperature of 550 °C, a weight hourly space velocity (WHSV) of oleic acid of 1 h^{-1}, and a TOS of 12 h. Liquid samples (collected in a 20 mL glass vial) and gas-phase samples (collected in a 5 L FlexFoil Plus sample bag with stainless steel fitting, part no. 207104, SKC Ltd.) were taken every 30 min through two parallel 3-stage condensation and separation systems by simultaneously switching the pneumatic Valves V11, V12, and V15 (Figure 1).

Catalyst Regeneration and Reuse. The used catalyst (termed as Used-*i* catalyst, where *i* represents the number of reaction-regeneration cycles) was unloaded from the reactor after cooling to room temperature under N_2 flow (50 mL min^{-1}). The oxidative regeneration of the used catalyst (placed in a 90 mL Haldenwanger porcelain crucible, product no. 10493081, Fisher Scientific Nederlands) was performed in a muffle furnace. The furnace temperature was programmed from room temperature to 680 °C in 10.7 h and maintained at 680 °C for 12 h, followed by cooling to room temperature in 10.7 h. The regenerated catalyst (termed as Regenerated-*i* catalyst, where *i* represents catalyst regenerated sequences in the muffle furnace) was placed in the reactor to determine the reusability of the H-ZSM-5/Al_2O_3 catalysts for the catalytic conversion of oleic acid. The protocol for evaluating the fresh catalyst was applied for testing the regenerated catalyst. In total, the regenerated catalyst was recycled 6 times, and thus the results for 7 cycles of reaction-regeneration are reported.

Product Analysis. The biphasic liquid products (organic and aqueous phase) collected in the 20 mL glass vials were diluted approximately 7 times with a stock solution (*ca.* 20,000 ppm of *n*-nonane in a mixed solvent containing THF and ethanol with a volume ratio of *ca.* 1 to 10) to prepare homogeneous samples for various off-line analyses. The mixtures were analyzed by GC-MS (6890/5973, Hewlett-Packard) and GC-FID (5890, Hewlett-Packard). Both GCs were equipped with a Rtx-1701 column (30 m × 0.25 mm × 0.25 μm, Restek). The relative response factors of the individual aromatics to the internal standard, *viz.*, *n*-nonane, were applied for the quantification of aromatics. The carbon, hydrogen, and oxygen contents in the samples were analyzed using a EuroEA3000 elemental analyzer (Eurovector). The water content in the samples was measured by Karl Fischer titration on a 702 SM Titrino potentiometric titrator (Metrohm). HYDRANAL 5 and HYDRANAL (Honeywell) were used as the titer and the solvent, respectively.

The gaseous products collected in the 5 L gas bags were analyzed by GC-TCD (5890, Hewlett-Packard) equipped with a CP-PoraBOND Q column (50 m × 0.53 mm × 10 μm, Varian) and an HP-Molsieve column (30 m × 0.53 mm × 50 μm, Agilent). Before and after the analyses of the gaseous products, the GC-TCD was pre- and post-calibrated with a standard reference gas mixture containing C_1−C_3, CO, CO_2, and N_2 (Product No. G322243, Westfalen AG).

The carbon yields of products, the selectivity of individual BTX components, and total BTX productivity were calculated using eqs 1−3. Catalyst lifetime is defined as the TOS when the yield of BTX was below the thermal threshold.

$$\text{Yield(\%, on carbon basis)} = \frac{\text{mol of carbon in the individual product}}{\text{mol of carbon in oleic acid feed}} \times 100 \quad (1)$$

$$\text{BTX selectivity(\%)} = \frac{\text{mol of individual BTX component produced}}{\text{mol of total BTX product}} \times 100 \quad (2)$$

$$\text{Total BTX productivity}(mg_{BTX} g_{catalyst}^{-1}) = \frac{\text{weight of BTX produced}}{\text{weight of catalyst loaded in the reactor}} \quad (3)$$

https://dx.doi.org/10.1021/acssuschemeng.0c06181
ACS Sustainable Chem. Eng. 2021, 9, 1128−1141

Catalyst Characterization. The fresh, used, and regenerated catalysts were ground into fine powders before analysis.

Physisorption experiments with N_2 and Ar were performed on an ASAP 2420 (Micromeritics) at 77 and 87 K, respectively. Before the measurements, the catalyst was degassed at 450 °C for 4 h. The specific surface area (S_{BET}) was calculated using the Brunauer–Emmett–Teller (BET) method.[54] The total pore volume (V_{pore}) was estimated by a single point N_2 desorption at P/P_0 of 0.98. The mesopore size distribution and volume ($V_{mesopore}$) were calculated according to the Barrett–Joyner–Halenda (BJH) method.[55] The micropore size distribution and volume ($V_{micropore}$) were obtained from Ar isotherms by applying the Non-Localized Density Functional Theory (NLDFT[56]).

Powder X-ray diffraction (XRD) spectra were collected on a D8 Advance Powder Diffractometer (Bruker, Germany) using Cu Kα radiation (λ = 1.5418 Å), which operated at 40 kV and 40 mA. The spectra were recorded by an LYNXEYE detector (1D mode) in a 2θ scan range of 5–50°. The relative crystallinity of the catalyst was calculated using eq 4, in which the height (H) of the peak at 2θ = 24.37° was applied (ASTM D5758-01 method).

$$\text{Relative crystallinity}(\%) = \frac{H_{\text{catalyst}}}{H_{\text{fresh catalyst}}} \times 100 \quad (4)$$

Transmission electron microscopy (TEM) images were taken on a Tecnai T20 transmission electron microscope (FEI), which is equipped with a Gatan model 626 cryo-stage working at 200 keV. Energy dispersive X-ray (EDX) analysis was carried out by an X-Max T80 SDD EDX Detector (Oxford). The catalyst was ultrasonically dispersed in ethanol and subsequently deposited on a carbon-coated copper grid.

Magic angle spinning (MAS) solid-state nuclear magnetic resonance (ssNMR) spectra were obtained on an AV-I 750 MHz spectrometer (Bruker) with a magnetic field of 17.6 T and a MAS rate of 54.74 kHz. For ^{27}Al and ^{29}Si MAS ssNMR spectra, chemical shifts were referenced to $Al(NO_3)_3$ and tetramethylsilane (TMS), respectively, and 1024 scans were recorded.

Temperature-programmed desorption of ammonia (NH_3-TPD) was performed on an AutoChem II (Micromeritic). The catalyst was pretreated by He (50 mL min^{-1}) at 550 °C for 1 h followed by cooling to 100 °C. An NH_3/He stream (1.0 vol %, 50 mL min^{-1}) was then introduced to adsorb NH_3 on the catalyst for 1 h. After purging by He (50 mL min^{-1}) for 1 h, the temperature was increased to 550 °C (10 °C min^{-1}) and maintained for 30 min. The desorbed NH_3 was detected by TCD, which was calibrated for NH_3 quantification.

Thermogravimetric analysis (TGA) was conducted on a TGA 4000 (PerkinElmer) using synthetic air (50 mL min^{-1}). The catalyst was loaded in a ceramic crucible and the temperature was programmed from 50 to 800 °C with a heating rate of 10 °C min^{-1}. The curve for the empty crucible (blank experiment) was also measured using the same protocol.

Elemental (carbon) analysis was carried out on a EuroEA3000 elemental analyzer (Eurovector). The standard reference (sulfanilamide, CAS No. 63–74–1) was supplied by Elemental Microanalysis Ltd.

RESULTS AND DISCUSSION

Pyrolysis of oleic acid without using a catalyst. The thermal pyrolysis of oleic acid was performed in the fixed bed reactor filled with quartz wool for a TOS of 2 h at 550 °C (Figure 1). The condensed products were collected every half hour. The liquid yield was 74.7 ± 0.9 wt % with an oxygen content of 7.8 ± 0.1 wt % (elemental analysis), indicating a deoxygenation degree of *ca.* 79.4%. The water content in the samples (Karl Fischer titration) was about 5.3 ± 0.1 wt %, indicating that *ca.* 31% of the bound oxygen in oleic acid was converted to H_2O. This is probably due to the dehydration[32,33] of oleic acid and intermediates thereof. GC-MS analysis of the liquid product (Table S1) shows that oleic acid (*ca.* 17.5 peak area%) is partly converted to a variety of olefins (heptadecene, 1-pentene, 1-heptene, 1,7-octadiene), cycloalkanes (methylcyclooctane), and acids (*n*-hexadecanoic acid and *n*-decanoic acid). BTX was not formed in the absence of a catalyst.

Fresh Catalyst Performance. The catalytic conversion of oleic acid (WHSV 1 h^{-1}) to bioaromatics over a fresh granular H-ZSM-5/Al_2O_3 catalyst (10 g loading) was continuously performed in a fixed bed reactor at a catalyst bed temperature of 550 °C, under atmospheric pressure for a TOS of 12 h. These reaction conditions (T, P, and WHSV) are selected based on a previous study by our group for the catalytic conversion of crude glycerol to bio-BTX.[18] The composition of the liquid product versus TOS was determined by off-line GC-FID analyses and shows that BTX formation becomes negligible after 6.5 h, indicating severe catalyst deactivation (*vide infra*). Oleic acid was typically not present in the liquid phase, indicating complete conversion. Only in the case where the catalyst is deactivated and minor amounts of BTX are formed a small amount of unconverted oleic acid is present in the liquid phase (*e.g.*, TOS of 12 h, *ca.* 3.8 peak area% of oleic acid, by GC-MS). The overall bioaromatics yield during catalyst lifetime is 20.7% (on carbon basis, Figure 2A) and 15.1

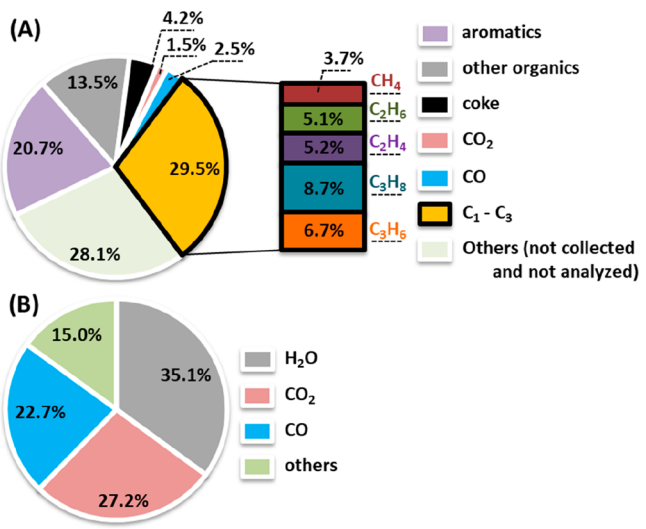

Figure 2. (A) Carbon balance and (B) oxygen balance for catalytic conversion of oleic acid over fresh H-ZSM-5/Al_2O_3 catalyst. Reaction conditions: catalyst particle size of 1.2–1.8 mm, catalyst loading of 10 g, catalyst bed temperature of 550 °C, atmospheric pressure, N_2 flow of 50 mL min^{-1}, and WHSV of oleic acid of 1 h^{-1}.

wt % (on a weight basis, Figure S2). The liquid product contains, besides BTX, also long-chain alkanes and alkenes, and fatty acids (*vide infra*) which account for about 13.5% of the carbon (equivalent to 19.7 wt %, Figure S2). Besides, gas-phase components like short hydrocarbons (C_1–C_3) are formed in a carbon yield of 29.5% (equivalent to 27.1 wt %, Figure S2) in combination with low amounts of CO (2.5%, on carbon basis, Figure 2A) and CO_2 (1.5%, on carbon basis, Figure 2A). The amount of coke deposited on the used catalyst is 4.2% on C basis (Figure 2A). The remaining 28.1% of carbon (Figure 2A) or 19.2% of mass (Figure S2) was not identified, though most is likely present in the form of residues that could not be recovered from the reactor system (*e.g.*, condensers and transfer lines, related to the small scale of the unit) and components which were not quantified by GC-TCD

https://dx.doi.org/10.1021/acssuschemeng.0c06181
ACS Sustainable Chem. Eng. 2021, 9, 1128–1141

and GC-FID (*e.g.*, C_4 hydrocarbons). The oxygen balance (Figure 2B) indicates that the bound oxygen in oleic acid is converted to H_2O (35.1%), CO_2 (27.2%), and CO (22.7%). This implies that three deoxygenation reactions, namely, dehydration, decarboxylation, and decarbonylation, occur at rather similar rates.

The yields for aromatics and gaseous products versus TOS are shown in Figures 3 and S3. Oleic acid conversion is

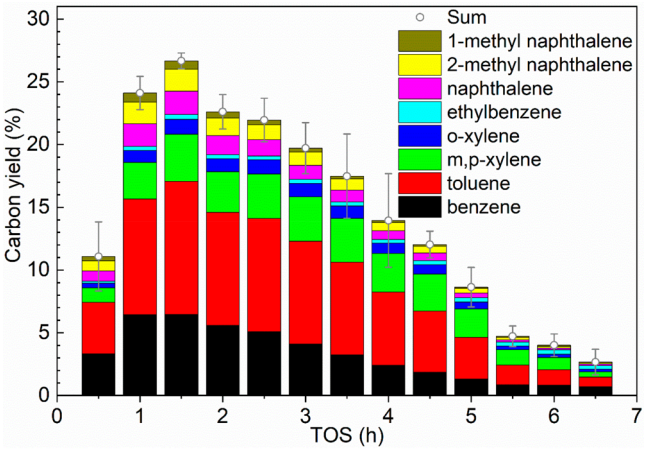

Figure 3. Carbon yields of aromatics versus TOS over fresh H-ZSM-5/Al_2O_3 catalysts. Reaction conditions: catalyst particle size of 1.2−1.8 mm, catalyst loading of 10 g, catalyst bed temperature of 550 °C, atmospheric pressure, N_2 flow of 50 mL min^{-1}, and WHSV of oleic acid of 1 h^{-1}.

quantitative at short TOS but not in a later stage when the yields of aromatics become low. The yields of all products at a TOS of 30 min (first sample) are rather low, most likely related to the start-up of the reactor. A peak carbon yield of aromatics (26.7%) was obtained at a TOS of 1.5 h. BTX are the major aromatic products (carbon yield of 22.0%), followed by naphthalene (carbon yield of 1.9%), 1- and 2-methyl-naphthalene (carbon yield of 1.7% and 0.7%), and ethyl-benzene (carbon yield of 0.4%). It is difficult to compare these yields with literature data as large differences in reaction conditions and reactor types are applied, which all affect the yields (Table 1). A further complication is that it is often unclear whether the peak yields or average yields are reported. Nevertheless, the peak yield and also the overall yield of aromatics in this study are in the range with those reported for rapeseed oil (*e.g.*, 22.5−26.8 wt %[36,39]), camelina seed oil (*e.g.*, 6.2 wt %[37]), soybean oil (*e.g.*, 24.5−25 wt %[36,38]), and palm oil (*e.g.*, 22 wt %[36]) (Table 1, entries 4−6). At prolonged TOS, the aromatics yield decreases gradually (Figure 3). After a TOS of 6.5 h, the carbon yield of aromatics dropped to 2.7% and was stable afterward (*e.g.*, 2.6% at TOS of 8 h). This number is close to the reported aromatics yield (<1.5 wt %) from rapeseed oil conversion without using a catalyst.[57] These results indicate that the catalyst was deactivated considerably after a TOS of 6.5 h. The total BTX productivity for the fresh catalyst over its lifetime is *ca.* 740 mg g^{-1} catalyst (Table 2). After 5 recycles, the cumulative BTX productivity is about 10 kg BTX kg^{-1} catalyst (Table 2). This number is still low when considering catalyst performance criteria (e.g., 1−100 ton product kg^{-1} catalyst)[58] for industrial processes. As such, further detailed studies using dedicated reactor configurations

Table 2. Performance of the Fresh and Regenerated H-ZSM-5/Al_2O_3 Catalysts

	peak carbon yield of BTX (%)	catalyst lifetime (h)	total BTX productivity (mg g^{-1} catalyst)
Fresh	22.0	6.5	740 (for lifetime of 6.5 h)
Regenerated-1	25.3	11	1280 (for lifetime of 11 h)
Regenerated-2	21.8	>12	1925 (for TOS of 12 h)
Regenerated-3	21.7	>12	1820 (for TOS of 12 h)
Regenerated-4	17.8	>12	1630 (for TOS of 12 h)
Regenerated-5	16.4	>12	1765 (for TOS of 12 h)
Regenerated-6	16.3	>24	1735 (for TOS of 12 h) (3025 for TOS of 24 h)

(*e.g.*, FCC alike) aiming to study hundreds of recycle/regeneration steps will be required.

Results for Seven Reaction-Regeneration Cycles. It has been shown in Fresh Catalyst Performance that the activity of the fresh H-ZSM-5/Al_2O_3 for BTX formation became very low after about 6.5 h TOS. Characterization of the used catalyst (*vide infra*) shows that catalyst deactivation is caused by severe coke deposition on the catalyst, resulting in a blockage of micropores and coverage of acidic sites. Several oxidative regeneration experiments using air were performed at a range of temperatures (600−680 °C) and times (4−12 h) to regenerate/reactivate the catalyst. Characterization of the regenerated catalyst (*vide infra*) indicated that most of the coke was removed after an oxidative regeneration in the air at 680 °C for 12 h. The regenerated catalyst was subjected to another experiment with oleic acid following the same protocol as for the fresh catalyst. BTX yield and selectivity versus TOS were considered to evaluate the performance of the regenerated catalyst. A total of 7 reaction-regeneration cycles were performed and the results are shown in Figure 4 and summarized in Table 2.

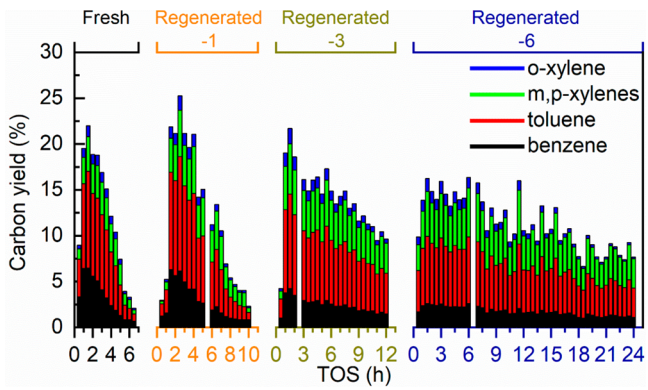

Figure 4. Carbon yields of aromatics versus TOS over fresh and regenerated H-ZSM-5/Al_2O_3 catalysts. Reaction conditions: catalyst particle size of 1.2−1.8 mm, catalyst loading of 10 g, catalyst bed temperature of 550 °C, atmospheric pressure, N_2 flow of 50 mL min^{-1}, and oleic acid feeding of 10 g h^{-1}.

The peak carbon BTX yield using the regenerated catalysts gradually decreased with the number of reaction-regeneration cycles (*e.g.*, 21.7% for Regenerated-3 catalyst vs 16.3% for Regenerated-7 catalyst, Figure 4 and Table 2). Interestingly, the regenerated catalyst lifetime was dramatically prolonged, *e.g.*, to at least 11 h for Regenerated-1 catalyst (Figure 4 and

https://dx.doi.org/10.1021/acssuschemeng.0c06181
ACS Sustainable Chem. Eng. 2021, 9, 1128−1141

Table 2), leading to significantly enhanced BTX productivity of *ca.* 1280 mg g^{-1} Regenerated-1 catalyst (Table 2). After 2 times of regeneration, the catalyst lifetime was even longer than the TOS used for the experiment (*viz.*, 12 h). As such, a longer TOS experiment for 24 h was performed. However, this experiment showed that the catalyst was still active for BTX (7.7% yield) after at TOF of 24 h. Nevertheless, the total BTX productivity was already 3 times higher than for the fresh catalyst (Table 2), showing the great potential of reusing the catalyst after regeneration for lowering the catalyst consumption.[58] In addition, it seems that after 4−5 cycles of reaction-regeneration, the regenerated catalysts perform similarly concerning BTX yield and selectivity (Figure S4), and total BTX productivity (Table 2, Regenerated-4, -5, and -6 catalysts). It suggests that the catalyst reaches a steady state after a certain number of reaction-regeneration cycles, which is typically also observed for FCC catalysts. These interesting observations differ for those obtained by the authors using glycerol as the feed over either an unmodified H-ZSM-5 zeolite catalyst (5 cycles of reaction-regeneration)[47] or a shaped H-ZSM-5/bentonite catalyst (11 cycles of reaction-regeneration),[18] where the catalyst lifetime was reduced with more regeneration cycles. These differences may be associated with the properties of the feed (*e.g.*, H/C_{eff} ratio) as well as the use of (different) binders.

In addition, of interest is the observation that the selectivity for the individual BTX components differs for the fresh and the regenerated catalysts (Figures 4 and S4). The selectivity of *m,p*-xylene was remarkably increased while a significant drop in benzene selectivity was observed. These findings imply a change in catalyst characteristics with the number of reaction-regeneration cycles (*vide infra*).

Catalyst Characterization for Fresh, Used, and Regenerated H-ZSM-5/Al_2O_3 Catalysts. To get insights into the changes in catalyst structure and morphology during a run and after regeneration, the fresh catalyst (Fresh), deactivated catalysts after the first (Used-1) and seventh (Used-7) reaction, and regenerated catalysts after the first (Regenerated-1) and seventh (Regenerated-7) regeneration were characterized by various techniques (*vide infra*).

Fresh H-ZSM-5/Al_2O_3 Catalyst. The H-ZSM-5/Al_2O_3 catalyst used in this study was made from an MFI-type ZSM-5 zeolite in the ammonium-form with a SiO_2/Al_2O_3 molar ratio of 28 and boehmite. The catalyst was shaped into granules at a particle size of 1.2−1.8 μm and calcined at 600 °C for 12 h. A TEM image including EDX mapping (Al and Si) of Fresh catalyst (Figure S5) shows the presence of H-ZSM-5 and Al_2O_3 particles. The quantified EDX analysis result (Figure S6) gives a SiO_2/Al_2O_3 molar ratio for the Fresh catalyst of ca. 2.1, which is close to the nominal value of 2.3 for a catalyst formulation with 60 wt % H-ZSM-5 and 40% boehmite.

N_2 adsorption−desorption isotherms for Fresh catalyst (Figure 5A-a) show a combination of type I (at low P/P_0) and type IV (at higher P/P_0) isotherms,[59] indicating the existence of microand mesopores. The BJH mesopore size distribution (Figure 5B-a) in pore size range 3−10 nm is in line with the formation of γ-Al_2O_3 from boehmite upon calcination at 500 °C.[60] The NLDFT micropore size distribution (Figure 5C-a) shows a sharp peak in the pore size range 0.4−0.6 nm (centered at 0.52 nm), in agreement with the micropore structure of an MFI-type zeolite (straight channels: *ca.* 0.54 × 0.56 nm^2, sinusoidal channels: *ca.* 0.51 × 0.55 nm^2)[61] and the reported micropore size distribution for

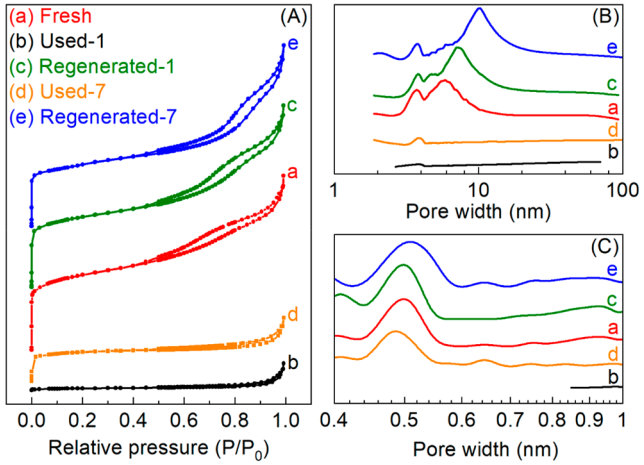

Figure 5. N_2 adsorption−desorption isotherms (A), BJH meso-pore size distribution (B), and NLDFT micropore size distribution (C) of fresh, used, and regenerated H-ZSM-5/Al_2O_3 catalysts.

H-ZSM-5 with a SiO_2/Al_2O_3 molar ratio of 23.[47] The specific surface area (S_{BET}) and pore volume (V_{pore}) of the Fresh catalyst are depicted in Table 3. The pore volume of Fresh catalyst (*ca.* 0.26 cm^3 g^{-1}) is much higher than the reported ones for H-ZSM-5 with a SiO_2/Al_2O_3 molar ratio of 23 (*ca.* 0.21 cm^3 g^{-1}[47]) and 32 (*ca.* 0.18 cm^3 g^{-1}[62]). This is most likely related to the contribution of the larger pore volume from the mesoporous Al_2O_3 compared to the microporous H-ZSM-5. These findings are in line with those by Verkleij et al.,[62] showing that the total pore volume of H-ZSM-5/Al_2O_3 catalyst increases with a higher proportion of an Al_2O_3 binder.

The XRD pattern of the Fresh catalyst (Figure 6a) shows two distinct diffraction peaks (hearts) at 2θ = *ca.* 7.9° and 8.9°, corresponding to the [011] and [200] planes of a typical MFI-type zeolite,[63] which is in line with the reported XRD pattern for H-ZSM-5 with a SiO_2/Al_2O_3 molar ratio of 23[18,47] and within the range 30−280.[64] Diffraction peaks from the Al_2O_3 matrix are hardly present in the H-ZSM-5/Al_2O_3 catalyst (Figure 6a), implying that the crystallinity of the γ-Al_2O_3 binder is by far lower than that of the ZSM-5 zeolite.[65]

^{27}Al MAS ssNMR spectrum of Fresh catalyst (Figure 7A-a) displays three peaks from Al atoms in different coordination environments. The two peaks at δ = *ca.* 68 and 11 ppm are in line with those reported for γ-Al_2O_3[66] and related to tetrahedrally and octahedrally coordinated Al, respectively. ^{27}Al MAS ssNMR spectra of ZSM-5 zeolites with different SiO_2/Al_2O_3 molar ratios (*e.g.*, 23[47] and 30−150[67]) typically display two peaks at δ = *ca.* 55 and 0 ppm, originating from a tetrahedrally coordinated framework Al (FAl) and an octahedrally coordinated extra-framework Al (EFAl).[68] However, only one peak (leftward diagonal down arrow) at δ = *ca.* 55 ppm from the ZSM-5 zeolite is observed for the fresh H-ZSM-5/Al_2O_3 (Figure 7A-a) and the peak at δ = *ca.* 0 ppm is absent. This might be due to the fact this peak is very weak and is overlapping with the intensive peak at δ = *ca.* 11 ppm for γ-Al_2O_3 matrix.[66] These findings are in agreement with ^{27}Al MAS ssNMR data reported in the literature for a related H-ZSM-5/Al_2O_3 catalyst.[69]

A ^{29}Si MAS ssNMR spectrum of the Fresh catalyst (Figure 7B-a) shows a sharp peak at δ = *ca.* −112 ppm and a shoulder (rightward diagonal down arrow) at δ = *ca.* −105 ppm,

https://dx.doi.org/10.1021/acssuschemeng.0c06181
ACS Sustainable Chem. Eng. 2021, 9, 1128−1141

Table 3. Relevant Properties of the Fresh, Used, and Regenerated Catalysts

catalyst	S_{BET}[a] ($m^2\ g^{-1}$)	V_{pore}[a] ($cm^3\ g^{-1}$)	NLDFT $V_{micropore}$[b] ($cm^3\ g^{-1}$)	relative crystallinity[c] (%)	acidity[d] (μmol NH_3 g^{-1} sample)	carbon content[e] (wt %)	coke content[f] (wt %)	T_M of DTG[f] (°C)	coking rate[f] ($g\ h^{-1}$)
Fresh	288	0.27	0.27	100	1051	-	-	-	-
Used-1	9	0.03	0.02	-	394	20.7	22.3	538	0.34
Regenerated-1	265	0.29	0.26	100	823	-	-	-	-
Used-7	110	0.09	0.09	-	166	19.2	20.4	569	0.085
Regenerated-7	235	0.28	0.26	69	376	-	-	-	-

[a]N_2 adsorption−desorption at 77 K. [b]Ar adsorption−desorption at 87 K. [c]XRD. [d]NH_3-TPD. [e]CHN elemental analysis. [f]TG-DTG.

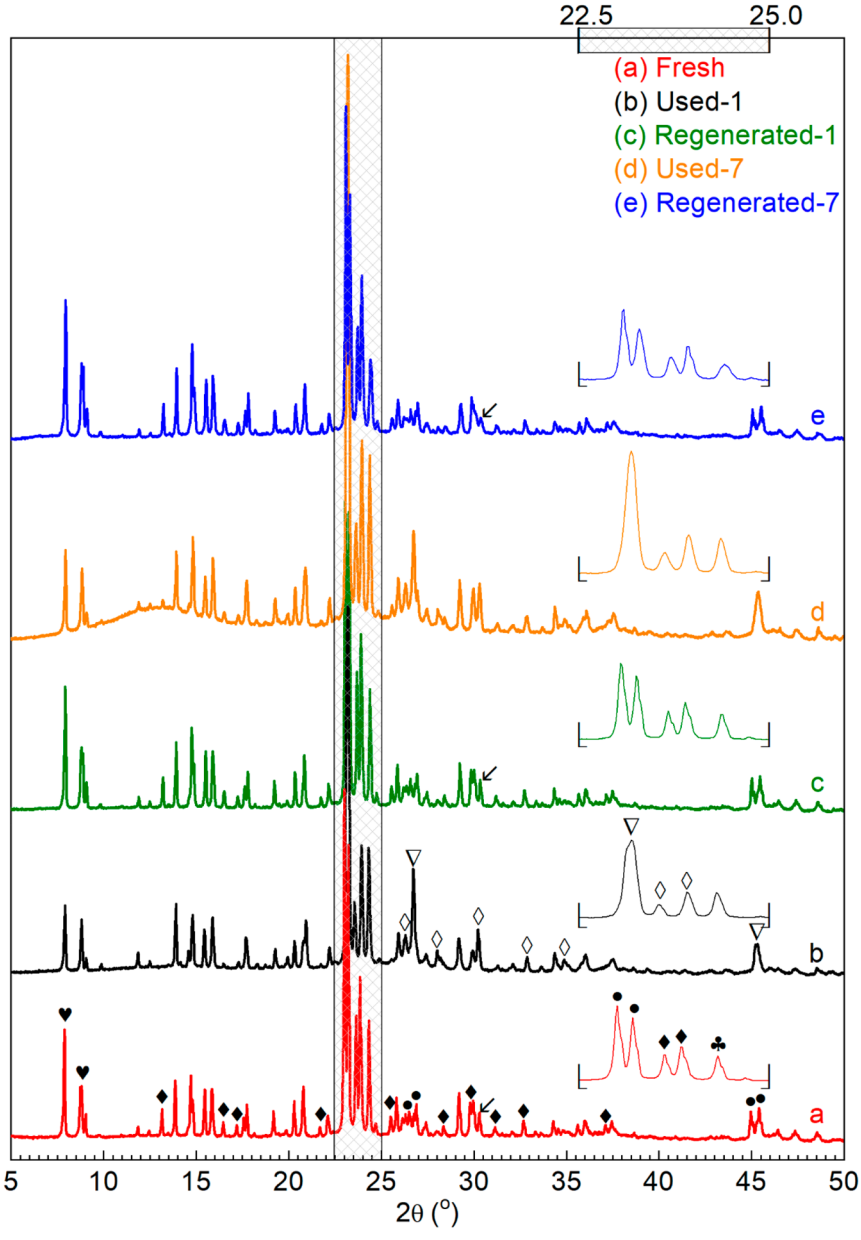

Figure 6. XRD patterns of fresh, used, and regenerated H-ZSM-5/Al_2O_3 catalysts.

corresponding to the Q4 linkages of Si (Si(4Si, 0Al) and Si(3Si, 1Al), respectively) in the ZSM-5 framework.[70,71]

The NH_3-TPD profile of the Fresh catalyst (Figure S7-a) shows a bimodal distribution. The broad peak at low-temperature peak (*ca.* 100−330 °C) reflects weak acid sites and the high-temperature peak (*ca.* 330−550 °C) is associated with strong acidic sites in the H-ZSM-5 zeolite.[72] Considering that the acidity of Al_2O_3 is considerably lower than that of the ZSM-5 zeolite,[73] the H-ZSM-5/Al_2O_3 catalyst mostly presents the acidity features of the H-ZSM-5 zeolite. This is well reflected by the shape of the NH_3-TPD profile, which is in line with that reported for ZSM-5 zeolites with different SiO_2/

https://dx.doi.org/10.1021/acssuschemeng.0c06181
ACS Sustainable Chem. Eng. 2021, 9, 1128−1141

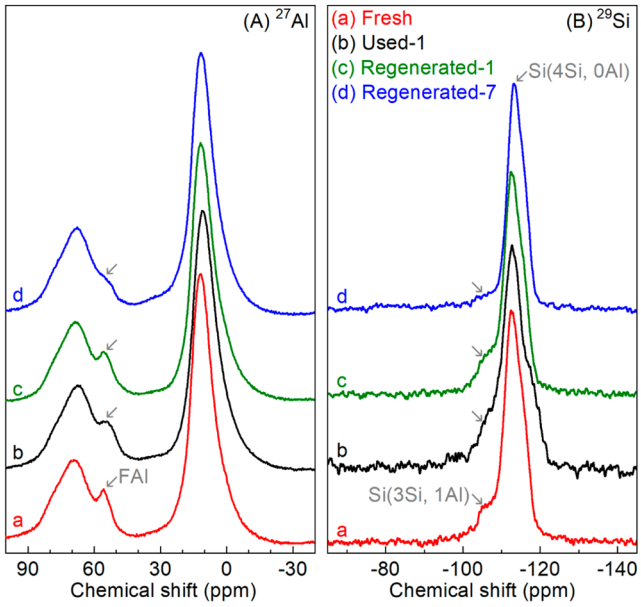

Figure 7. ^{27}Al and ^{29}Si MAS ssNMR spectra of fresh, used, and regenerated H-ZSM-5/Al_2O_3 catalysts.

Al_2O_3 molar ratios (*e.g.*, 23[47] and 30–280[74]). Besides, the quantified acidity is *ca.* 730 μmol NH_3 g^{-1} Fresh catalyst (Table 3), which is also very close to that for the catalyst formulation used here (60%) when considering the acidity of pure ZSM-5 zeolite with a SiO_2/Al_2O_3 molar ratio of 23 (*ca.* 1320[74] and 1464[47] μmol NH_3 g^{-1} catalyst) and 30 (*ca.* 1120[74] and 1260[75] μmol NH_3 g^{-1} catalyst).

Used H-ZSM-5/Al_2O_3 Catalyst. It was shown that the fresh and regenerated H-ZSM-5/Al_2O_3 catalysts became inactive for BTX synthesis after a certain TOS. A TGA (Figure 8) of Used-1 and Used-7 catalyst shows the presence of considerable amounts of coke on the catalyst (*ca.* 22.0 and 20.4 wt % of coke (Table 3) after first reaction and seventh reaction). The presence of coke was confirmed by CHN elemental analyses (Table 3), showing that 20.7 wt % of the carbon feed was present on Used-1 and 19.2 wt % on Used-7.

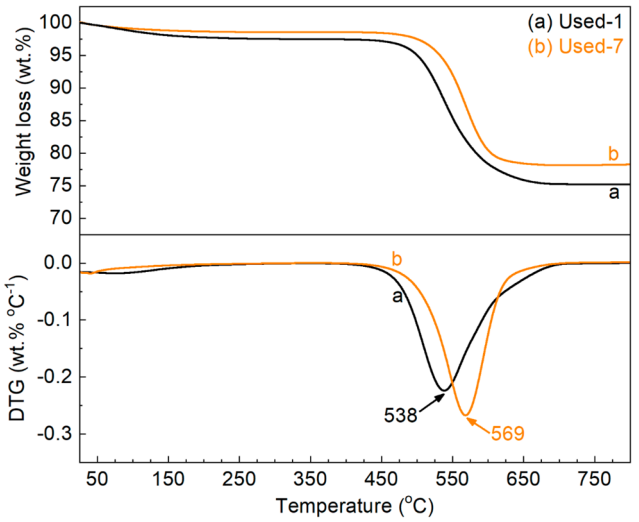

Figure 8. TG-DTG curves of used H-ZSM-5/Al_2O_3 catalysts.

Quantitative EDX analyses also confirm the carbon content in the two used catalysts (*e.g.*, 19.6 wt % for Used-1 (Figure S8-a) and 18.8 wt % for Used-7 (Figure S8-c)), in line with elemental analyses data (Table 3). EDX mappings of Used-1 (Figures S8-a and S9) and Used-7 (Figures S8-c and S10) catalysts also clearly show the presence of coke on the used catalyst. Interestingly, the coke is not distributed evenly, and relatively higher concentrations of carbon (Figures S9-b and S10-b) are observed in the particles with a higher concentration of Al (Figures S9-c and S10-c). This indicates that more coke is formed in the Al_2O_3 particles within the matrix than in the H-ZSM-5 zeolite. A possible explanation is the presence of mesopores in Al_2O_3 (Figure 5B-a), giving rise to larger pore volume,[62] and therefore, it can accommodate more coke than the micropores in the H-ZSM-5 zeolite (Figure 5C-a). Besides, compared to H-ZSM-5, Al_2O_3 has lower acidity[73] and a higher chance for thermal cracking, leading to enhanced coke formation.

XRD patterns of Used-1 (Figure 6b) and Used-7 (Figure 6d) catalysts display some additional major (∇) and minor (◇) diffraction peaks, which are not present in XRD patterns of Fresh (Figure 6a), Regenerated-1 (Figure 6c), and Regenerated-7 (Figure 6e) catalysts and are thus assigned to the coke deposited on the used catalysts. The three major diffraction peaks (∇) at 2θ = *ca.* 23.2°, 26.7°, and 45.3° (Figure 6b and d) overlap the twin diffraction peaks (●) for H-ZSM-5 zeolite (Figure 6a) at 2θ = *ca.* 23.1° and 23.2°, 26.6°, and 26.8°, and 45.0° and 45.4°. This indicates that a highly crystalline coke is formed on the catalyst, likely related to carbon species with a graphitic structure. Due to coke deposition, the intensity of some diffraction peaks (◆), assigned to the various planes of H-ZSM-5 zeolite (Figure 6a), is reduced dramatically for the used catalysts (Figure 6b and d).

Moreover, the textural properties of Used-1 (Figure 5) and Used-7 (Figure 5) catalysts also differ considerably when compared to the fresh catalyst. For Used-1 catalyst, which showed a very low activity for aromatics production, surface area (9 m^2 g^{-1}) and pore volume (0.03 cm^3 g^{-1}) were reduced considerably (Table 3). Compared to Used-1 catalyst, Used-7 catalyst, which was still active for producing aromatics, has a higher surface area and pore volume (Table 3), being 38% and 33% of those for the Fresh catalyst.

Severe coking also led to a considerable decrease in acidity for the Used-1 and Used-7 catalysts (Table 3). Strong acid sites, generally associated with Brønsted acid sites, are hardly detected for Used-1 (Figure S6-b) and Used-7 (Figure S7-d). A higher acidity was found for the partially deactivated Used-7 catalyst when compared to the fully deactivated Used-1 catalyst (Table 3).

For several liquid biomass sources (*e.g.*, pyrolysis bio-oil and crude glycerol), irreversible catalyst deactivation (besides reversible coke formation) was found for the catalytic pyrolysis over ZSM-5 zeolite-based catalyst. This is generally associated with the dealumination of the ZSM-5 framework due to the presence of water in the gas phase.[18,76,77] Detailed catalyst studies on H-ZSM-5 catalyst for glycerol conversion to bioaromatics and after several reaction-regeneration cycles[47] by the authors have revealed that the dealumination of the H-ZSM-5 zeolite mainly occurs during the reaction and not during regeneration and is likely due to the formation of significant amounts of water/steam during catalytic pyrolysis. However, in this study, negligible dealumination was observed

https://dx.doi.org/10.1021/acssuschemeng.0c06181
ACS Sustainable Chem. Eng. 2021, 9, 1128–1141

for Used-1 catalyst. This is indicated by the MAS ssNMR spectra for the Used-1 catalyst, showing only slightly changed peak intensities (Peak leftward diagonal down arrow, Figure 7A-b) and Q4(3Si, 1Al) (Peak rightward diagonal down arrow, Figure 7B-b) for FAl linkages. This lower level of dealumination when using oleic acid is most likely due to the lower amount of oxygen in oleic acid (11.3 vs 52. wt % in glycerol), which upon reaction leads to less steam formation when compared to glycerol.

Regenerated H-ZSM-5/Al_2O_3 Catalyst. Analyses of the spent catalyst show that coke formation occurs to a considerable extent during the reaction. This coke will cover active sites and block pores in the H-ZSM-5/Al_2O_3 catalyst, leading to partial (*e.g.*, Used-7 catalyst) and severe (*e.g.*, Used-1 catalyst) deactivation. DTG analyses (Figure 7) of Used-1 and Used-7 catalysts provide information on the theoretical minimum temperature (T_M, Table 3) required to remove the coke by an oxidative regeneration. In practice, a higher temperature is often required to shorten oxidation time.

Several regeneration trails were carried out at a temperature range of 600−680 °C for a regeneration time of 4−12 h under air in a muffle furnace. EDX analyses of Regenerated-1 and Regenerated-7 catalysts (Figure S8-b and d) show that >98% of the coke is removed from the regenerated catalysts after oxidation at 680 °C for 12 h. This is also reflected in the disappearance of diffraction peaks (∇ and ◇, Figure 6b) assigned for coke in XRD patterns of Regenerated-1 and Regenerated-7 catalysts (Figure 6c and e).

After regeneration, the surface area and pore volume of Regenerated-1 catalyst (Table 3) were fully restored, as well as the mesopore (Figure 5B-c) and micropore (Figure 5C-c) size distributions. Regenerated-1 catalyst shows the same XRD pattern as Fresh catalyst (Figure 6c vs a). The relative crystallinity of Regenerated-1 catalyst, calculated by dividing the diffraction peak (black club, Figure 6) height for Regenerated-1 catalyst by that for Fresh catalyst, is about 100% (Table 3). Besides, no obvious dealumination of the H-ZSM-5 framework was observed on Regenerated-1 catalyst, as indicated by marginal changes in MAS ssNMR spectra of ^{27}Al (Peak leftward diagonal down arrow, Figure 7A-c) and ^{29}Si (Peak rightward diagonal down arrow, Figure 7B-c) for Regenerated-1 catalyst compared with those for the Fresh catalyst. However, a drop of acidity (Table 3) and especially the strong acidity (Figure S7-c) is observed for Regenerated-1 catalyst. In a recent study from us, we have shown that catalytic upgrading of a pyrolysis vapor of glycerol over an H-ZSM-5 zeolite in a fixed bed reactor follows a "conversion-zone migration" mode, and a small layer of the catalyst with sufficient active sites (*e.g.*, acidity and microporosity) can maintain a good BTX yield. In this study, we also observe that the decrease in acidity barely affects the peak BTX yield over Regenerated-1 catalyst compared with Fresh catalyst (Figure 4 and Table 2). Also of high interest is the experimentally observed prolonged catalyst lifetime for Regenerated-1 catalyst when compared to the Fresh one (Figure 4 and Table 2). A possible explanation is the reduced acidity of Regenerated-1, which may slow down the side reactions for coke precursor formation. Consequently, after first reaction-regeneration cycle, the textural properties and crystalline structure of the H-ZSM-5/Al_2O_3 catalyst were well preserved, hardly any dealumination of the H-ZSM-5 framework occurred, while the acidity was decreased. These catalyst characteristics promoted a longer catalyst lifetime without affecting the peak BTX yield, resulting in a higher total BTX productivity for Regenerated-1 catalyst.

With more cycles of reaction-regeneration, the performance of the regenerated catalysts (Figure 4) changes (lower peak yields, longer lifetime), and this is also reflected in the catalyst characteristics (*e.g.*, textural, crystalline, and acidic features). After 7 reaction-regeneration cycles, higher levels of dealumination of the H-ZSM-5 framework were detected. This is clearly shown by the dramatic decrease in peak intensity for peaks corresponding to FAl (Peak leftward diagonal down arrow in Figure 7A-d) and Si(3Si, 1Al) (Peak rightward diagonal down arrow in Figure 7B-d) in ^{27}Al and ^{29}Si MAS ssNMR spectra for Regenerated-7 catalyst compared with those for Fresh catalyst. This is probably due to prolonged high-temperature exposure of the catalyst to steam (formed by dehydration of oleic acid, see above) and possibly also due to the use of oleic acid, particularly when considering that organic acids may mildly dealuminate ZSM-5.[78] The framework defects caused by dealumination may also affect the textural and crystalline structure of H-ZSM-5. The latter was indeed observed by a decreased relative crystallinity (*ca.* 31%) for Regenerated-7 catalyst (Figure 6 and Table 3), along with a significant reduction in the diffraction peak (leftward diagonal down arrow in Figure 6) at 2θ = *ca.* 30.3° (assigned to [612] plane of H-ZSM-5, JCPDS card No. 00−044−0002). The specific surface area and pore volume for the Regenerated-7 catalyst were also reduced to *ca.* 82% of the values for Fresh catalyst (Table 3). Moreover, the acidity was also affected, and only *ca.* 52% of the acidity of the Fresh catalyst was preserved for Regenerated-7 catalyst (Table 3). The degradation of these important catalyst characteristics caused a decrease in the peak carbon yield of BTX from 22.5% over the Fresh catalyst to 16.3% over the Regenerated-6 catalyst (Figure 4 and Table 2). Of great interest is the observation that the selectivity of *m,p*-xylene was dramatically increased (Figure S4) and catalyst lifetime was also remarkably prolonged. This higher *m,p*-xylene selectivity is associated with a decrease in benzene selectivity. A possible explanation is a reduction in the rate of dealkylation of xylenes to benzene due to a reduced acidity of the catalyst.[47] The prolonged catalyst lifetime for multiple regenerated catalysts might be due to the inhibition of side reactions (*e.g.*, coking) over the regenerated catalyst with reduced acidity, reflected by a much lower average coking rate for Regenerated-6 catalyst compared with that for Fresh catalyst (Table 3).

When considering the trend in performance of the regenerated catalysts, it appears that the peak carbon yield of BTX, total BTX production, and the selectivity of individual BTX components becomes about constant after 4 cycles of reaction-regeneration, indicating that the catalysts change into a sort of steady-state catalyst (Figures 4 and S4, and Table 2). However, additional reaction-regeneration cycles combined with further characterization of the regenerated catalysts need to be performed to substantiate this hypothesis. Nevertheless, the above catalyst characterization studies and the demonstration of seven reaction-regeneration cycles show that passivation of the very active fresh H-ZSM-5 zeolite-based catalyst (*e.g.*, by dealkylation[79] and silylation[80]) may be an interesting option to explore in future studies on biomass conversion to bioaromatics.

Reaction Network for Oleic Acid Conversion to Aromatics. The catalytic conversion of oleic acid over the H-ZSM-5/Al_2O_3 catalyst produces condensable liquid organic

https://dx.doi.org/10.1021/acssuschemeng.0c06181
ACS Sustainable Chem. Eng. 2021, 9, 1128−1141

products (*e.g.*, BTX and heavy aromatics), noncondensable gaseous products (*e.g.*, low hydrocarbons, H_2, CO, and CO_2), and also solid coke on the catalyst (Figure 2). Besides the products shown in Figure 3, there are several unquantified components, which also need to be considered to study the reaction network for oleic acid conversion to aromatics. It has been shown in Figure 3 that a peak carbon yield of aromatics was obtained at a TOS of 1.5 h. With longer TOS, the carbon yields for aromatics and low hydrocarbons decrease gradually (Figure 3). The catalyst showed very low activity (likely thermal) for aromatics production after TOS of 6.5 h, which was also confirmed by characterization of the used catalyst (*e.g.*, negligible surface area, pore-volume, and acidity) after TOS of 12 h. Therefore, two representative liquid products (*viz.*, collected at TOS of 1.5 and 12 h) from one run were selected and further analyzed by GC-MS to qualify the distribution of products from the catalytic conversion of oleic acid and the one when using a deactivated catalyst. The GC-MS spectra of these two products (Figure 9) differ considerably. The product obtained at a TOS of 1.5 h (from a catalytic experiment, Figure 9a) consisted of BTX and naphthalenes (major, also quantified in Figure 3), as well as some other aromatics (minor), such as substituted benzenes (ethyl methylbenzenes, trimethylbenzenes, ethyl dimethylbenzenes, and methyl propenylbenzenes) and polycyclic aromatic hydrocarbons (PAHs, anthracene, phenanthrene, and their analogues). However, the product at TOS of 12 h, when the catalyst shows a low activity for BTX formation (Figure 9b) consist of a mixture of linear saturated and unsaturated hydrocarbons with carbon chain lengths of 6−16 (major) and cyclic hydrocarbons (minor) as well, and carboxylic acids including unconverted oleic acid. This product distribution is in good accordance with the reported ones for the thermal conversion of oleic acid at elevated temperatures,[81,82] and the results for the thermal oleic acid reaction performed in this study (see above). As such, we assume that these products are the precursors for aromatic formation on the active, acidic sites of the zeolite catalyst.

Oleic acid is known to be preferentially converted to long-chain alkanes and alkenes (*e.g.*, C_{16}, Figure 9b) by a McLafferty rearrangement[83] under thermal cracking conditions (Scheme S1). These long-chain hydrocarbons are readily cracked to various intermediates such as reactive carbenium ions, carbonium ions, or free radicals,[84,85] which are further converted to hydrocarbons with shorter carbon chain length (*e.g.*, C_6−C_{16} in Figure 9b and C_1−C_3 in Figure S3). The unconverted oleic acid (Figure 9b) and monocarboxylic acids derived thereof (*e.g.*, nonanoic acid and decanoic acid, Figure 9b) can also be converted to hydrocarbons by deoxygenation reactions,[86] resulting in the formation of CO, CO_2, and H_2O (Figure 2B). These hydrocarbons are further cracked over the Lewis and Brønsted acidic sites of the H-ZSM-5/Al_2O_3 catalyst to form a hydrocarbon pool (*e.g.*, C_2−C_6). BTX (major) and heavy aromatics (minor) are subsequently formed from the hydrocarbon pool (Figure 2) by various reactions (Friedel−Crafts alkylations, Diels−Alder reactions, dehydrogenations, oligomerizations, cyclization)[87] over the acidic sites in the H-ZSM-5 zeolite microchannels.[88] Dealkylation of already formed aromatics also occurs and affects the BTX selectivity with TOS.[47] This is well reflected by the higher *m,p*-xylene selectivity, and the decreased benzene selectivity with TOS (Figure S4), which is likely due to the reduced acidity of the catalysts due to coking. Besides the desired aromatics (BTX),

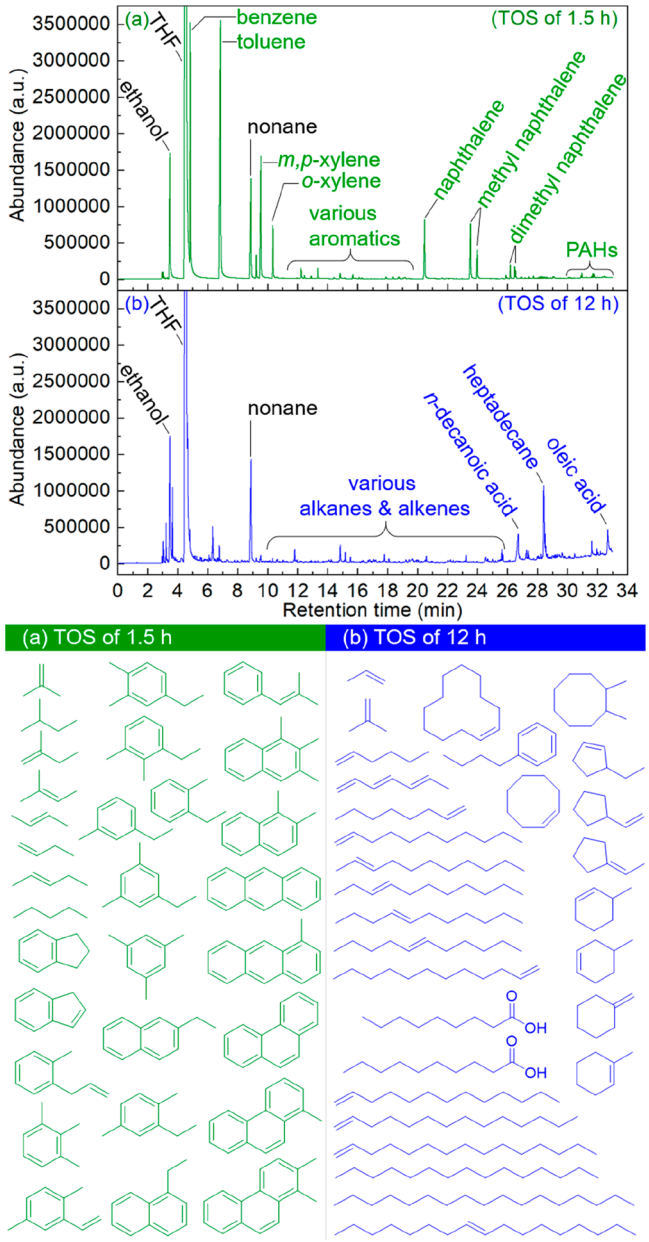

Figure 9. GC-MS spectra of the liquid products at a TOS of (a) 1.5 h and (b) 12 h.

PAHs are also formed (Figure 9a), which are known coke precursors and may lead to a reduction in catalyst activity after longer TOS (*e.g.*, 6.5 h for Fresh catalyst, Figure 3).

CONCLUSIONS

It has been shown above that oleic acid has good potential for bioaromatics synthesis via an *ex situ* catalytic pyrolysis approach. A commercially produced granular H-ZSM-5/Al_2O_3 catalyst showed a good catalyst performance for this purpose at 550 °C and atmospheric pressure, and a peak carbon yield of BTX of 22.7% was found with a total BTX production of 1000 mg g^{-1} catalyst for a catalyst lifetime of 6.5 h. Catalyst lifetime was on the order of hours due to coke formation on the catalyst surface. However, coke is easily removed by an oxidative regeneration procedure, which was confirmed by 7 reaction-regeneration cycles. Although catalyst characteristics (textural properties, crystallinity, framework,

https://dx.doi.org/10.1021/acssuschemeng.0c06181
ACS Sustainable Chem. Eng. 2021, 9, 1128−1141

and acidity) imply some degradation of the catalyst after 7 times of regeneration, the total BTX production was enhanced to >3025 mg g^{-1} catalyst, owing to a dramatically prolonged catalyst lifetime of >24 h. The BTX selectivity also changed upon the number of reaction-regeneration cycles, and particularly, the selectivity to *m,p*-xylene increased at the expense of benzene, rationalized by a reduction in the total acidity upon the number of reaction-regeneration cycles. It also appears that the regenerated H-ZSM-5/Al_2O_3 catalyst reaches a sort of steady-state after 4−5 reaction-regeneration cycles, though further confirmation with additional cycles of reaction-regeneration test and catalyst characterization is required.

Thus, this study using a model fatty acid has provided new insights into reaction and (reversible and irreversible) catalyst deactivation mechanisms for BTX synthesis. It shows that both reversible (by coking) as well as irreversible catalyst deactivation (by dealumination, resulting in a loss in acidity) occurs. Irreversible catalyst deactivation is not detrimental for catalyst performance and actually, BTX productivity is positively affected when using a recycled/regenerated catalyst. The results are useful to understand the potential of bioliquids containing such fatty acids (*e.g.*, crude glycerol) and more complex crude and used vegetable (as well as the animal and fish) oils for BTX synthesis over zeolite-based catalysts. This study also indicates that fresh catalyst is too active (too acidic) and leads to high coking rates, and thus reduced catalyst lifetime. As such, passivation of an H-ZSM-5 zeolite catalyst (*e.g.*, by dealumination or by alkylation/silylation) may lead to improved performance.

■ ASSOCIATED CONTENT

Supporting Information

The Supporting Information is available free of charge at https://pubs.acs.org/doi/10.1021/acssuschemeng.0c06181.

Pricing for BTX, mass balances, carbon yields of gaseous products versus TOS, carbon yields of aromatics and selectivities of the individual BTX versus TOS, catalyst characterizations (TEM-EDX, NH_3-TPD, and Elemental (Al, Si, and C) maps), and a proposed reaction network for BTX formation (PDF)

■ AUTHOR INFORMATION

Corresponding Author

Hero Jan Heeres − *Green Chemical Reaction Engineering, Engineering and Technology Institute Groningen, University of Groningen, 9747 AG Groningen, The Netherlands;* orcid.org/0000-0002-1249-543X; Email: h.j.heeres@rug.nl

Authors

Songbo He − *Green Chemical Reaction Engineering, Engineering and Technology Institute Groningen, University of Groningen, 9747 AG Groningen, The Netherlands;* orcid.org/0000-0002-5001-6620

Frederike Gerda Hiltje Klein − *Green Chemical Reaction Engineering, Engineering and Technology Institute Groningen, University of Groningen, 9747 AG Groningen, The Netherlands*

Thomas Sjouke Kramer − *Green Chemical Reaction Engineering, Engineering and Technology Institute Groningen, University of Groningen, 9747 AG Groningen, The Netherlands*

Anshu Chandel − *Green Chemical Reaction Engineering, Engineering and Technology Institute Groningen, University of Groningen, 9747 AG Groningen, The Netherlands*

Zhuorigebatu Tegudeer − *Green Chemical Reaction Engineering, Engineering and Technology Institute Groningen, University of Groningen, 9747 AG Groningen, The Netherlands*

Andre Heeres − *Hanze University of Applied Sciences, 9747 AS Groningen, The Netherlands*

Complete contact information is available at: https://pubs.acs.org/10.1021/acssuschemeng.0c06181

Notes

The authors declare no competing financial interest.

■ ACKNOWLEDGMENTS

Financial support from Nederlandse Organisatie voor Wetenschappelijk Onderzoek (NWO) is acknowledged (NWO-LIFT program, Grant No. 731.016.401). We thank N. Schenk, I. Muizebelt, and P. Imhof from BIOBTX B.V. for stimulating discussions, and Dr. Karthick Sai Sankar Gupta (NMR Facility at Leiden University), and Dr. M.C.A. Stuart (Electron Microscopy Facility at the University of Groningen) for their contributions on MAS ssNMR and HR-TEM-EDX analyses.

■ REFERENCES

(1) BTX (Benzene Toluene And Xylene) Market. https://www.reportsanddata.com/report-detail/btx-benzene-toluene-and-xylene-market (accessed 31 October, 2020).

(2) Lok, C. M.; Van Doorn, J.; Almansa, G. A. Promoted ZSM-5 catalysts for the production of bio-aromatics, a review. *Renewable Sustainable Energy Rev.* **2019**, *113*, 1−11.

(3) BioBTX, Pilot plans BioBTX officially opened on Zernike campus on 13th September 2018. www.biobtx.com (accessed 5th August, 2020).

(4) Anellotech, Bio-TCat for Renewable Chemicals & Fuels. https://www.anellotech.com/bio-tcat%E2%84%A2-renewable-chemicals-fuels (accessed 5th August, 2020).

(5) Carlson, T. R.; Cheng, Y. T.; Jae, J.; Huber, G. W. Production of green aromatics and olefins by catalytic fast pyrolysis of wood sawdust. *Energy Environ. Sci.* **2011**, *4* (1), 145−161.

(6) Chen, H.; Shi, X.; Liu, J.; Jie, K.; Zhang, Z.; Hu, X.; Zhu, Y.; Lu, X.; Fu, J.; Huang, H.; Dai, S. Controlled synthesis of hierarchical ZSM-5 for catalytic fast pyrolysis of cellulose to aromatics. *J. Mater. Chem. A* **2018**, *6* (42), 21178−21185.

(7) Yang, M. F.; Shao, J. G.; Yang, H. P.; Chen, Y. Q.; Bai, X. W.; Zhang, S. H.; Chen, H. P. Catalytic pyrolysis of hemicellulose for the production of light olefins and aromatics over Fe modified ZSM-5 catalysts. *Cellulose* **2019**, *26* (15), 8489−8500.

(8) Yang, M.; Shao, J.; Yang, Z.; Yang, H.; Wang, X.; Wu, Z.; Chen, H. Conversion of lignin into light olefins and aromatics over Fe/ZSM-5 catalytic fast pyrolysis: Significance of Fe contents and temperature. *J. Anal. Appl. Pyrolysis* **2019**, *137*, 259−265.

(9) Foster, A. J.; Jae, J.; Cheng, Y.-T.; Huber, G. W.; Lobo, R. F. Optimizing the aromatic yield and distribution from catalytic fast pyrolysis of biomass over ZSM-5. *Appl. Catal., A* **2012**, *423*, 154−161.

(10) Carlson, T. R.; Tompsett, G. A.; Conner, W. C.; Huber, G. W. Aromatic production from catalytic fast pyrolysis of biomass-derived feedstocks. *Top. Catal.* **2009**, *52* (3), 241−252.

(11) Jing, Y. X.; Guo, Y.; Xia, Q. N.; Liu, X. H.; Wang, Y. Q. Catalytic production of value-added chemicals and liquid fuels from lignocellulosic biomass. *Chem.* **2019**, *5* (10), 2520−2546.

(12) Kabir, G.; Hameed, B. H. Recent progress on catalytic pyrolysis of lignocellulosic biomass to high-grade bio-oil and bio-chemicals. *Renewable Sustainable Energy Rev.* **2017**, *70*, 945−967.

(13) Li, Z. L.; Lepore, A. W.; Salazar, M. F.; Foo, G. S.; Davison, B. H.; Wu, Z. L.; Narula, C. K. Selective conversion of bio-derived ethanol to renewable BTX over Ga-ZSM-5. *Green Chem.* **2017**, *19* (18), 4344−4352.
(14) Vispute, T. P.; Zhang, H. Y.; Sanna, A.; Xiao, R.; Huber, G. W. Renewable chemical commodity feedstocks from integrated catalytic processing of pyrolysis oils. *Science* **2010**, *330* (6008), 1222−1227.
(15) Cheng, Y. T.; Jae, J.; Shi, J.; Fan, W.; Huber, G. W. Production of renewable aromatic compounds by catalytic fast pyrolysis of lignocellulosic biomass with bifunctional Ga/ZSM-5 catalysts. *Angew. Chem., Int. Ed.* **2012**, *51* (6), 1387−1390.
(16) Rezaei, P. S.; Shafaghat, H.; Daud, W. Production of green aromatics and olefins by catalytic cracking of oxygenate compounds derived from biomass pyrolysis: A review. *Appl. Catal., A* **2014**, *469*, 490−511.
(17) Heeres, A.; Schenk, N.; Muizebelt, I.; Blees, R.; De Waele, B.; Zeeuw, A. J.; Meyer, N.; Carr, R.; Wilbers, E.; Heeres, H. J. Synthesis of bio-aromatics from black liquors using catalytic pyrolysis. *ACS Sustainable Chem. Eng.* **2018**, *6* (3), 3472−3480.
(18) He, S.; Muizebelt, I.; Heeres, A.; Schenk, N. J.; Blees, R.; Heeres, H. J. Catalytic pyrolysis of crude glycerol over shaped ZSM-5/bentonite catalysts for bio-BTX synthesis. *Appl. Catal., B* **2018**, *235*, 45−55.
(19) Satyarthi, J. K.; Chiranjeevi, T.; Gokak, D. T.; Viswanathan, P. S. An overview of catalytic conversion of vegetable oils/fats into middle distillates. *Catal. Sci. Technol.* **2013**, *3* (1), 70−80.
(20) Ooi, Y. S.; Zakaria, R.; Mohamed, A. R.; Bhatia, S. Catalytic conversion of fatty acids mixture to liquid fuel and chemicals over composite microporous/mesoporous catalysts. *Energy Fuels* **2005**, *19* (3), 736−743.
(21) Bayat, A.; Sadrameli, S. M. Conversion of canola oil and canola oil methyl ester (CME) to green aromatics over a HZSM-5 catalyst: a comparative study. *RSC Adv.* **2015**, *5* (36), 28360−28368.
(22) Mo, N.; Pennebacker, J.; Savage, P. E. Hydrocarbon chemicals from hydrothermal processing of renewable oils over HZSM-5. *Biomass Convers. Biorefin.* **2017**, *7* (4), 437−443.
(23) Atabani, A. E.; Silitonga, A. S.; Ong, H. C.; Mahlia, T. M. I.; Masjuki, H. H.; Badruddin, I. A.; Fayaz, H. Non-edible vegetable oils: A critical evaluation of oil extraction, fatty acid compositions, biodiesel production, characteristics, engine performance and emissions production. *Renewable Sustainable Energy Rev.* **2013**, *18*, 211−245.
(24) Carpenter, D. L.; Lehmann, J.; Mason, B. S.; Slover, H. T. Lipid composition of selected vegetable oils. *J. Am. Oil Chem. Soc.* **1976**, *53* (12), 713−718.
(25) Hammond, E. W. Vegetable oils | Types and properties. In *Encyclopedia of Food Sciences and Nutrition*, 2nd ed., Caballero, B., Ed.; Academic Press: Oxford, 2003; pp 5899−5904. DOI: 10.1016/B0-12-227055-X/01225-6.
(26) Orsavova, J.; Misurcova, L.; Ambrozova, J. V.; Vicha, R.; Mlcek, J. Fatty acids composition of vegetable oils and its contribution to dietary energy intake and dependence of cardiovascular mortality on dietary intake of fatty acids. *Int. J. Mol. Sci.* **2015**, *16* (6), 12871−12890.
(27) Dupain, X.; Costa, D. J.; Schaverien, C. J.; Makkee, M.; Moulijn, J. A. Cracking of a rapeseed vegetable oil under realistic FCC conditions. *Appl. Catal., B* **2007**, *72* (1−2), 44−61.
(28) Zheng, Y.; Wang, J.; Liu, C.; Lu, Y.; Lin, X.; Li, W.; Zheng, Z. Efficient and stable Ni-Cu catalysts for ex situ catalytic pyrolysis vapor upgrading of oleic acid into hydrocarbon: Effect of catalyst support, process parameters and Ni-to-Cu mixed ratio. *Renewable Energy* **2020**, *154*, 797−812.
(29) Benson, T. J.; Hernandez, R.; White, M. G.; French, W. T.; Alley, E. E.; Holmes, W. E.; Thompson, B. Heterogeneous cracking of an unsaturated fatty acid and reaction intermediates on H+ZSM-5 catalyst. *Clean: Soil, Air, Water* **2008**, *36* (8), 652−656.
(30) Mo, N.; Savage, P. E. Hydrothermal catalytic cracking of fatty acids with HZSM-5. *ACS Sustainable Chem. Eng.* **2014**, *2* (1), 88−94.
(31) Mo, N.; Tandar, W.; Savage, P. E. Aromatics from saturated and unsaturated fatty acids via zeolite catalysis in supercritical water. *J. Supercrit. Fluids* **2015**, *102*, 73−79.
(32) Bielansky, P.; Weinert, A.; Schönberger, C.; Reichhold, A. Gasoline and gaseous hydrocarbons from fatty acids via catalytic cracking. *Biomass Convers. Biorefin.* **2012**, *2* (1), 53−61.
(33) Revellame, E. D.; Holmes, W. E.; Benson, T. J.; Forks, A. L.; French, W. T.; Hernandez, R. Parametric study on the production of renewable fuels and chemicals from phospholipid-containing biomass. *Top. Catal.* **2012**, *55* (3−4), 185−195.
(34) Hilten, R.; Speir, R.; Kastner, J.; Das, K. C. Production of aromatic green gasoline additives via catalytic pyrolysis of acidulated peanut oil soap stock. *Bioresour. Technol.* **2011**, *102* (17), 8288−8294.
(35) Tamiyakul, S.; Anutamjarikun, S.; Jongpatiwut, S. The effect of Ga and Zn over HZSM-5 on the transformation of palm fatty acid distillate (PFAD) to aromatics. *Catal. Commun.* **2016**, *74*, 49−54.
(36) Bielansky, P.; Weinert, A.; Schonberger, C.; Reichhold, A. Catalytic conversion of vegetable oils in a continuous FCC pilot plant. *Fuel Process. Technol.* **2011**, *92* (12), 2305−2311.
(37) Zhao, X.; Wei, L.; Cheng, S.; Huang, Y.; Yu, Y.; Julson, J. Catalytic cracking of camelina oil for hydrocarbon biofuel over ZSM-5-Zn catalyst. *Fuel Process. Technol.* **2015**, *139*, 117−126.
(38) Zheng, Z.; Wang, J.; Wei, Y.; Liu, X. J.; Yu, F. W.; Ji, J. B. Effect of La-Fe/Si-MCM-41 catalysts and CaO additive on catalytic cracking of soybean oil for biofuel with low aromatics. *J. Anal. Appl. Pyrolysis* **2019**, *143*, 1−11.
(39) Idem, R. O.; Katikaneni, S. P. R.; Bakhshi, N. N. Catalytic conversion of canola oil to fuels and chemicals: Roles of catalyst acidity, basicity and shape selectivity on product distribution. *Fuel Process. Technol.* **1997**, *51* (1−2), 101−125.
(40) Ramos, R.; Garcia, A.; Botas, J. A.; Serrano, D. P. Enhanced production of aromatic hydrocarbons by rapeseed oil conversion over Ga and Zn modified ZSM-5 catalysts. *Ind. Eng. Chem. Res.* **2016**, *55* (50), 12723−12732.
(41) Wang, F.; Zheng, Y. W.; Huang, Y. B.; Yang, X. Q.; Xu, G. F.; Kang, J.; Liu, C.; Zheng, Z. F. Optimizing catalytic pyrolysis of rubber seed oil for light aromatics and anti deactivation of ZSM-5. *J. Anal. Appl. Pyrolysis* **2017**, *126*, 180−187.
(42) Zhao, X. H.; Wei, L.; Julson, J.; Qiao, Q. Q.; Dubey, A.; Anderson, G. Catalytic cracking of non-edible sunflower oil over ZSM-5 for hydrocarbon bio-jet fuel. *New Biotechnol.* **2015**, *32* (2), 300−312.
(43) Zhao, X. H.; Wei, L.; Cheng, S. Y.; Julson, J.; Anderson, G.; Muthukumarappan, K.; Qiu, C. L. Development of hydrocarbon biofuel from sunflower seed and sunflower meat oils over ZSM-5. *J. Renewable Sustainable Energy* **2016**, *8* (1), 1−17.
(44) Wang, J.; Zhong, Z. P.; Ding, K.; Zhang, B.; Deng, A. D.; Min, M.; Chen, P.; Ruan, R. Successive desilication and dealumination of HZSM-5 in catalytic conversion of waste cooking oil to produce aromatics. *Energy Convers. Manage.* **2017**, *147*, 100−107.
(45) Fegade, S.; Tande, B.; Kubatova, A.; Seames, W.; Kozliak, E. Novel two-step process for the production of renewable aromatic hydrocarbons from triacylglycerides. *Ind. Eng. Chem. Res.* **2015**, *54* (39), 9657−9665.
(46) Kadrmas, C.; Khambete, M.; Kubatova, A.; Kozliak, E.; Seames, W. Optimizing the production of renewable aromatics via crop oil catalytic cracking. *Processes* **2015**, *3* (2), 222−234.
(47) He, S.; Zuur, K.; Santosa, D. S.; Heeres, A.; Liu, C.; Pidko, E.; Heeres, H. J. Catalytic conversion of glycerol over an unmodified H-ZSM-5 zeolite to bio-based aromatics. *Appl. Catal., B* **2021**, *281*, 1−14.
(48) Veerkamp, J. H.; Mulder, I.; Van Deenen, L. L. M. Comparison of the fatty acid composition of lipids from different animal tissues including some tumours. *Biochim. Biophys. Acta* **1962**, *57* (1), 299−309.
(49) Ackman, R. G. Characteristics of the fatty acid composition and biochemistry of some fresh-water fish oils and lipids in comparison with marine oils and lipids. *Comp. Biochem. Physiol.* **1967**, *22* (3), 907−922.

https://dx.doi.org/10.1021/acssuschemeng.0c06181
ACS Sustainable Chem. Eng. 2021, 9, 1128−1141

(50) Gruger, E. H.; Stansby, M. E.; Nelson, R. W. Fatty acid composition of oils from 21 species of marine fish freshwater fish + shellfish. *J. Am. Oil Chem. Soc.* **1964**, *41* (10), 662−667.
(51) Xie, M.; Li, Y.; Etim, U. J.; Lou, H.; Xing, W.; Wu, P.; Liu, X.; Bai, P.; Yan, Z. Enhanced catalytic performance of the FCC catalyst with an alumina matrix modified by the zeolite Y structure-directing agent. *Ind. Eng. Chem. Res.* **2019**, *58* (14), 5455−5463.
(52) Iisa, K.; French, R. J.; Orton, K. A.; Budhi, S.; Mukarakate, C.; Stanton, A. R.; Yung, M. M.; Nimlos, M. R. Catalytic pyrolysis of pine over HZSM-5 with different binders. *Top. Catal.* **2016**, *59* (1), 94−108.
(53) Whiting, G. T.; Meirer, F.; Mertens, M. M.; Bons, A. J.; Weiss, B. M.; Stevens, P. A.; de Smit, E.; Weckhuysen, B. M. Binder effects in SiO_2- and Al_2O_3-bound zeolite ZSM-5-based extrudates as studied by microspectroscopy. *ChemCatChem* **2015**, *7* (8), 1312−1321.
(54) Brunauer, S.; Emmett, P. H.; Teller, E. Adsorption of gases in multimolecular layers. *J. Am. Chem. Soc.* **1938**, *60* (2), 309−319.
(55) Barrett, E. P.; Joyner, L. G.; Halenda, P. P. The determination of pore volume and area distributions in porous substances. 1. Computations from nitrogen isotherms. *J. Am. Chem. Soc.* **1951**, *73* (1), 373−380.
(56) Micromeretics, Model # 251, Ar@87-Zeolites, H-form, NLDFT. In *Micromeretics*: USA, 2017.
(57) Buzetzki, E.; Sidorová, K.; Cvengrošová, Z.; Kaszonyi, A.; Cvengroš, J. The influence of zeolite catalysts on the products of rapeseed oil cracking. *Fuel Process. Technol.* **2011**, *92* (8), 1623−1631.
(58) Lange, J.-P. Catalysis for biorefineries − performance criteria for industrial operation. *Catal. Sci. Technol.* **2016**, *6* (13), 4759−4767.
(59) Sing, K. S. W.; Everett, D. H.; Haul, R. A. W.; Moscou, L.; Pierotti, R. A.; Rouquerol, J.; Siemieniewska, T. Reporting physisorption data for gas/solid systems with special reference to the determination of surface area and porosity. *Pure Appl. Chem.* **1985**, *57* (4), 603−619.
(60) Hu, F.; Wu, X.; Wang, Y. M.; Lai, X. Y. Ultrathin gamma-Al_2O_3 nanofibers with large specific surface area and their enhanced thermal stability by Si-doping. *RSC Adv.* **2015**, *5* (67), 54053−54058.
(61) Olson, D. H.; Kokotailo, G. T.; Lawton, S. L.; Meier, W. M. Crystal structure and structure-related properties of ZSM-5. *J. Phys. Chem.* **1981**, *85* (15), 2238−2243.
(62) Verkleij, S. P.; Whiting, G. T.; Esclapez, S. P.; Mertens, M. M.; Bons, A. J.; Burgers, M.; Weckhuysen, B. M. Operando micro-spectroscopy on ZSM-5 containing extrudates during the oligomerization of 1-hexene. *Catal. Sci. Technol.* **2018**, *8* (8), 2175−2185.
(63) Treacy, M. M. J.; Higgins, J. B. MFI - ZSM-5, Calcined. In *Collection of simulated xrd powder patterns for zeolites* , 5th ed.; Elsevier Science B.V.: Amsterdam, 2007; pp 278−279. DOI: 10.1016/B978-044453067-7/50604-3.
(64) Sapi, A.; Kashaboina, U.; Abrahamne, K. B.; Gomez-Perez, J. F.; Szenti, I.; Halasi, G.; Kiss, J.; Nagy, B.; Varga, T.; Kukovecz, A.; Konya, Z. Synergetic of Pt Nanoparticles and H-ZSM-5 Zeolites for Efficient CO_2 Activation: Role of Interfacial Sites in High Activity. *Front. Mater.* **2019**, *6*, 1−12.
(65) Scheibler, J. R.; Santos, E. R. F.; Barbosa, A. S.; Rodrigues, M. G. F. Performance of zeolite membrane (ZSM-5/gamma-Alumina) in the oil/water separation process. *Desalin. Water Treat.* **2015**, *56* (13), 3561−3567.
(66) Samain, L.; Jaworski, A.; Eden, M.; Ladd, D. M.; Seo, D.-K.; Javier Garcia-Garcia, F.; Haussermann, U. Structural analysis of highly porous γ-Al_2O_3. *J. Solid State Chem.* **2014**, *217*, 1−8.
(67) Rodríguez-González, L.; Hermes, F.; Bertmer, M.; Rodríguez-Castellón, E.; Jiménez-López, A.; Simon, U. The acid properties of H-ZSM-5 as studied by NH_3-TPD and ^{27}Al-MAS-NMR spectroscopy. *Appl. Catal., A* **2007**, *328* (2), 174−182.
(68) Ramesh, K.; Jie, C.; Han, Y. F.; Borgna, A. Synthesis, characterization, and catalytic activity of phosphorus modified H-ZSM-5 catalysts in selective ethanol dehydration. *Ind. Eng. Chem. Res.* **2010**, *49* (9), 4080−4090.
(69) Magomedova, M.; Galanova, E.; Davidov, I.; Afokin, M.; Maximov, A. Dimethyl ether to olefins over modified ZSM-5 based catalysts stabilized by hydrothermal treatment. *Catalysts* **2019**, *9* (5), 1−19.
(70) Yu, Z. W.; Li, S. H.; Wang, Q.; Zheng, A. M.; Jun, X.; Chen, L.; Deng, F. Bronsted/Lewis Acid Synergy in H-ZSM-5 and H-MOR Zeolites Studied by H-1 and Al-27 DQ-MAS Solid-State NMR Spectroscopy. *J. Phys. Chem. C* **2011**, *115* (45), 22320−22327.
(71) Hartanto, D.; Yuan, L. S.; Sari, S. M.; Sugiarso, D.; Murwarni, I. K.; Ersam, T.; Prasetyoko, D.; Nur, H. The use of the combination of FTIR, pyridine adsorption, ^{27}Al AND ^{29}Si MAS NMR to determine the bronsted and lewis acidic sites. *J. Teknol.* **2016**, *78* (6), 223−228.
(72) Al-Dughaither, A. S.; de Lasa, H. HZSM-5 zeolites with different SiO_2/Al_2O_3 ratios. Characterization and NH_3 desorption kinetics. *Ind. Eng. Chem. Res.* **2014**, *53* (40), 15303−15316.
(73) Zhokh, A. A.; Trypolskyi, A. I.; Strizhak, P. E. Effect of H-ZSM-5/Al_2O_3 Catalyst Acidity on the Conversion of Methanol. *Theor. Exp. Chem.* **2017**, *53* (4), 276−282.
(74) Engtrakul, C.; Mukarakate, C.; Starace, A. K.; Magrini, K. A.; Rogers, A. K.; Yung, M. M. Effect of ZSM-5 acidity on aromatic product selectivity during upgrading of pine pyrolysis vapors. *Catal. Today* **2016**, *269*, 175−181.
(75) Lónyi, F.; Valyon, J. On the interpretation of the NH_3-TPD patterns of H-ZSM-5 and H-mordenite. *Microporous Mesoporous Mater.* **2001**, *47* (2), 293−301.
(76) Eschenbacher, A.; Jensen, P. A.; Henriksen, U. B.; Ahrenfeldt, J.; Li, C. X.; Duus, J. O.; Mentzel, U. V.; Jensen, A. D. Impact of ZSM-5 deactivation on bio-oil quality during upgrading of straw derived pyrolysis vapors. *Energy Fuels* **2019**, *33* (1), 397−412.
(77) Iliopoulou, E. F.; Stefanidis, S.; Kalogiannis, K.; Psarras, A. C.; Delimitis, A.; Triantafyllidis, K. S.; Lappas, A. A. Pilot-scale validation of Co-ZSM-5 catalyst performance in the catalytic upgrading of biomass pyrolysis vapours. *Green Chem.* **2014**, *16* (2), 662−674.
(78) Farahani, S. H.; Alavi, S. M.; Falamaki, C. Improved performance of HZSM-5 for the ethylbenzene/xylene isomerization reaction under industrial operating conditions. *RSC Adv.* **2017**, *7* (54), 34012−34022.
(79) Triantafillidis, C. S.; Vlessidis, A. G.; Nalbandian, L.; Evmiridis, N. P. Effect of the degree and type of the dealumination method on the structural, compositional and acidic characteristics of H-ZSM-5 zeolites. *Microporous Mesoporous Mater.* **2001**, *47* (2−3), 369−388.
(80) Chen, W.-H.; Bauer, F.; Bilz, E.; Freyer, A.; Huang, S.-J.; Lai, C.-S.; Liu, S.-B.; van Steen, E.; Claeys, M.; Callanan, L. H. Acidity characterization of H-ZSM-5 catalysts modified by pre-coking and silylation. *Stud. Surf. Sci. Catal.* **2004**, *154*, 2269−2274, DOI: 10.1016/S0167-2991(04)80485-3.
(81) Omidghane, M.; Jenab, E.; Chae, M.; Bressler, D. C. Production of renewable hydrocarbons by thermal cracking of oleic acid in the presence of water. *Energy Fuels* **2017**, *31* (9), 9446−9454.
(82) Asomaning, J.; Mussone, P.; Bressler, D. C. Thermal deoxygenation and pyrolysis of oleic acid. *J. Anal. Appl. Pyrolysis* **2014**, *105*, 1−7.
(83) Kubatova, A.; Geetla, A.; Casey, J.; Linnen, M. J.; Seames, W. S.; Smoliakova, I. P.; Kozliak, E. I. Cleavage of Carboxylic Acid Moieties in Triacylglycerides During Non-Catalytic Pyrolysis. *J. Am. Oil Chem. Soc.* **2015**, *92* (5), 755−767.
(84) Abbot, J. Catalytic cracking of long-chain paraffins and olefins on HY zeolite. *J. Catal.* **1990**, *124* (2), 548−552.
(85) Rangarajan, S.; Bhan, A.; Daoutidis, P. Rule-based generation of thermochemical routes to biomass conversion. *Ind. Eng. Chem. Res.* **2010**, *49* (21), 10459−10470.
(86) Sembiring, K. C.; Aunillah, A.; Minami, E.; Saka, S. Renewable gasoline production from oleic acid by oxidative cleavage followed by decarboxylation. *Renewable Energy* **2018**, *122*, 602−607.
(87) Das, J.; Bhat, Y. S.; Halgeri, A. B.; Rao, T. S. R. P.; Dhar, G. M. Aromatization of C_4-C_6 hydrocarbons to benzene, toluene and para xylene over pore size controlled ZnO-HZSM-5 zeolite. *Stud. Surf. Sci. Catal.* **1998**, *113*, 447−453, DOI: 10.1016/S0167-2991(98)80318-2.
(88) Derouane, E. G.; Gabelica, Z. A novel effect of shape selectivity - molecular traffic control in zeolite ZSM-5. *J. Catal.* **1980**, *65* (2), 486−489.

https://dx.doi.org/10.1021/acssuschemeng.0c06181
ACS Sustainable Chem. Eng. 2021, 9, 1128−1141